PROTEINS: Structure, Function, and Genetics 9:153–173 (1991)

RESEARCH ARTICLES

A Metal-Mediated Hydride Shift Mechanism for Xylose Isomerase Based on the 1.6 Å *Streptomyces rubiginosus* Structures With Xylitol and D-Xylose

Marc Whitlow, Andrew J. Howard, Barry C. Finzel, Thomas L. Poulos, Evon Winborne, and Gary L. Gilliland

Department of Protein Engineering, Genex Corporation, 16020 Industrial Dr., Gaithersburg, Maryland 20877

ABSTRACT **The crystal structure of recombinant *Streptomyces rubiginosus* D-xylose isomerase (D-xylose keto-isomerase, EC 5.3.1.5) solved by the multiple isomorphous replacement technique has been refined to $R = 0.16$ at 1.64 Å resolution. As observed in an earlier study at 4.0 Å (Carrell et al., J. Biol. Chem. 259: 3230–3236, 1984), xylose isomerase is a tetramer composed of four identical subunits. The monomer consists of an eight-stranded parallel β-barrel surrounded by eight helices with an extended C-terminal tail that provides extensive contacts with a neighboring monomer. The active site pocket is defined by an opening in the barrel whose entrance is lined with hydrophobic residues while the bottom of the pocket consists mainly of glutamate, aspartate, and histidine residues coordinated to two manganese ions.**

The structures of the enzyme in the presence of $MnCl_2$, the inhibitor xylitol, and the substrate D-xylose in the presence and absence of $MnCl_2$ have also been refined to $R = 0.14$ at 1.60 Å, $R = 0.15$ at 1.71 Å, $R = 0.15$ at 1.60 Å, and $R = 0.14$ at 1.60 Å, respectively. Both the ring oxygen of the cyclic α-D-xylose and its C1 hydroxyl are within hydrogen bonding distance of NE2 of His-54 in the structure crystallized in the presence of D-xylose. Both the inhibitor, xylitol, and the extended form of the substrate, D-xylose, bind such that the C2 and C4 OH groups interact with one of the two divalent cations found in the active site and the C1 OH with the other cation. The remainder of the OH groups hydrogen bond with neighboring amino acid side chains.

A detailed mechanism for D-xylose isomerase is proposed. Upon binding of cyclic α-D-xylose to xylose isomerase, His-54 acts as the catalytic base in a ring opening reaction. The ring opening step is followed by binding of D-xylose, involving two divalent cations, in an extended conformation. The isomerization of D-xylose to D-xylulose involves a metal-mediated 1,2-hydride shift. The final step in the mechanism is a ring closure to produce α-D-xylulose. The ring closing is the reverse of the ring opening step. This mechanism accounts for the majority of xylose isomerase's biochemical properties, including (1) the lack of solvent exchange between the 2-position of D-xylose and the 1-pro-R position of D-xylulose, (2) the chemical modification of histidine and lysine, (3) the pH vs. activity profile, and (4) the requirement for two divalent cations in the mechanism.

Key words: crystallographic, manganese, ring opening, X-ray

INTRODUCTION

The enzymatic isomerization of D-xylose to D-xylulose (Fig. 1) by D-xylose isomerase (EC 5.3.1.5) from *Pseudomonas hydrophila* was first described by Hochster and Watson in 1953[1] and in more detail in 1954.[2] Xylose isomerase is also capable of converting D-glucose to D-fructose. In both reactions a C1 proton is transferred to C2 in the ketose to aldose direction. The principal industrial use of xylose isomerase is the production of high fructose corn syrup (HFCS), involving the conversion of D-glucose to D-fructose.[3,4] In the United States 370 million bushels of corn were used in the production of HFCS in 1987.[5] Xylose isomerase is also used for ethanol production, in which the principal agricultural residue, xylose, is converted to xylulose by xylose isomerase and then to ethanol by fermentation.[6] Thus, there is considerable interest in understanding both the catalytic and structural details of this important industrial enzyme.

Received March 8, 1990; revision accepted August 30, 1990.

Address reprint requests to Marc Whitlow, Department of Protein Engineering, Genex Corporation, 16020 Industrial Drive, Gaithersburg, MD 20877.

Present address (B.C.F.): Physical and Analytical Chemistry, Upjohn Co., Kalamazoo, MI 49001.

Present address (T.L.P., E.W., G.L.G.): Center for Advanced Research in Biotechnology of the Maryland Biotechnology Institute, University of Maryland, Shady Grove, 9600 Gudelsky Drive, Rockville, MD 20850.

Present address (G.L.G.): Center for Chemical Technology, National Institute of Standards and Technology, Gaithersburg, MD 20899.

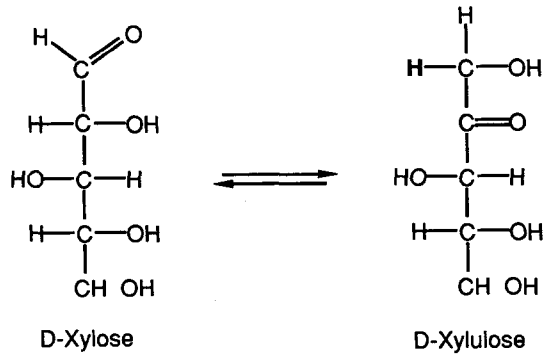

Fig. 1. The enzymatic reaction of xylose isomerase, the conversion of D-xylose to D-xylulose. 1-pro-R position of D-xylulose is shown in bold.

The chemical conversion of D-xylose to D-xylulose or of D-glucose to D-fructose is a subset of the Lobry de Bruyn–Alberda van Ekenstein transformation reaction.[7–9] Wohl and Neuberg[10] first proposed that the aldose–ketose isomerization proceeds through an enediol intermediate. These transformations can be either acid or base catalyzed. The base-catalyzed transformations of D-glucose to D-fructose show solvent exchange of the C1–C2 hydrogen.[11] These results suggest that an enediol intermediate is involved in these base-catalyzed transformations. Gleason and Barker[12] have shown a lack of solvent exchange in the base-catalyzed synthesis of D-ribose from D-arabinose and that enolization is not an obligatory first step in this rearrangement. The acid-catalyzed transformations between D-glucose and D-fructose[13] and between D-xylose and D-xylulose[14] do not show hydrogen exchange with the solvent. Since an enediol intermediate would exchange with the solvent, Ramchander and Feather[14] proposed a hydride shift or conducted tour mechanism. The lack of hydrogen exchange with solvent is also observed for the enzymatic reaction.

Xylose isomerase has been shown to transfer a proton from the 2-position of D-xylose (or D-glucose) to the 1-pro-R position of D-xylulose (or D-fructose) without exchange with solvent,[15,16] suggesting a hydride shift mechanism. We will show that Schray and Rose[17] correctly predicted the conformation around the C1–C2 bond in the binding of D-xylose to xylose isomerase, and incorrectly predicted the use of a catalytic base. Xylose isomerase is specific for α-D-xylose or α-D-glucose but not their enantiomorphs β-D-xylose or β-D-glucose.[17] α-D-Fructose is the product of the enzymatic conversion of α-D-glucose by xylose isomerase.[18] The affinities for D-xylose, D-xylulose, D-glucose, and D-fructose are 33, 18, 250, and 200 mM, respectively. The catalytic pH optimum of most xylose isomerase enzymes is around 8.5. The enzyme becomes active with the deprotonation of a group with a pK_a of 6.5 and protonation of a group with a pK_a of 9.5.[19] Both histidine and lysine have been implicated in the catalytic mechanism by chemical modification.[20] We will show that both of these residues are involved in the binding and catalysis of D-xylose by xylose isomerase.

Xylose isomerase is a metal ion dependent enzyme. Mg^{2+}, Co^{2+}, and Mn^{2+} activate the enzyme, whereas Ni^{2+}, Ca^{2+}, Ba^{2+}, Zn^{2+}, Cu^{2+}, and Hg^{2+} do not.[19,21] After dialysis against EDTA for 24 hr the enzyme has no activity.[19,22] The stability of the enzyme also depends on the amount and type of divalent metal ion present.[23] By Scatchard analysis the enzyme is shown to bind eight Co^{2+} per tetramer or two Co^{2+} per monomer.[22,24] Callens et al.[23] showed that the *Streptomyces violaceoruber* enzyme has less than 10% of its activity with one equivalent of Co^{2+} per monomer and has over 75% of its activity with two equivalents of Co^{2+} per monomer. The present work demonstrates that two metal ions are directly involved in the binding of D-xylose and proposes a hydride shift mechanism in which both metal ions are required.

When examining the structures of xylose isomerase and proposing a mechanism the following biochemical observations should be kept in mind. (1) Xylose isomerase is specific for the α anomers of D-xylose, D-xylulose, D-glucose, and D-fructose. (2) Both histidine and lysine have been implicted in the mechanism. (3) Two divalent cations are needed for xylose isomerase to be fully active. (4) The C1–C2 proton does not show exchange with solvent, suggestive of a hydride shift mechanism. A mechanism involving an enediol intermediate would require a base to transfer the C1–C2 proton and an environment to protect the proton from exchange with solvent. In contrast, a hydride shift mechanism does not need a catalytic base to transfer the C1–C2 proton and may or may not need protection of the proton against solvent exchange. Both mechanisms require a way to transfer the hydroxyl proton from O1 to D-xylose to O2 of D-xylulose.

Carrell et al. have reported structures at 1.9 Å of xylose isomerase with xylitol, D-xylose, and a substrate analog that is a suicide inactivator.[25] Based on the conformation of D-xylose and the reaction of the suicide inactivator, they have concluded that His-54 is the catalytic base responsible for transfering the C2 proton of D-xylose to the C1 of D-xylulose, involving an enediol intermediate. Their proposed mechanism does not account for a number of biochemical observations: (1) only one divalent cation is involved in their proposed mechanism, where as Callens et al. showed two are needed for full activity.[23] (2) A lysine is not involved in their proposed mechanism; Hoschle et al. showed by chemical modification that a lysine is involved in the mechanism.[20] (3) If His-54 is the catalytic base, we believe the proton would show exchange with solvent, because there are a number of solvent mole-

TABLE I. Crystallization Conditions

Data set	Metals	Substrate/inhibitor	Buffer/percipitant
Native	0.5 mM $MgCl_2$		50 mM HEPES, pH 7.0, 17% ammonium sulfate
$MnCl_2$	10 mM $MnCl_2$ 0.5 mM $MgCl_2$		50 mM HEPES, pH 7.0, 17% ammonium sulfate
Xylitol	0.5 mM $MgCl_2$	50 mM xylitol	50 mM HEPES, pH 7.0, 17% ammonium sulfate
Xylose	0.5 mM $MgCl_2$	40 mM D-xylose	50 mM HEPES, pH 7.0, 17% ammonium sulfate
Xylose + $MnCl_2$	50 mM $MnCl_2$ 0.5 mM $MgCl_2$	40 mM D-xylose	50 mM HEPES, pH 7.0, 17% ammonium sulfate

cules in close proximity. Recently, Collyer and Blow have suggested that Carrell et al.[25] have obtained a mixture of the cyclic and extended forms of D-xylose and that the suicide inactivator is not a good model for the binding of a closed-ring substrate.[26] We, like Collyer and Blow,[26] believe that a hydride shift mechanism is operating in xylose isomerase.

The present work describes the multiple isomorphous replacement (MIR) structure solution and refinement of xylose isomerase from *Streptomyces rubiginosus* at 1.64 Å. Based on biochemical data,[6] X-ray studies at 4.0 Å resolution,[27] and the DNA sequence,[28] the enzyme from *Streptomyces rubiginosus* is known to be a tetramer composed of identical monomers containing 388 residues with a calculated molecular weight of 43,232 each.[28] The 4.0 Å crystal structure demonstrated that the xylose isomerase monomer is formed by an eight-stranded parallel β-barrel surrounded by eight helices with the active site situated in a pocket near the center of the barrel.[27] In addition, the refined structures of D-xylose isomerase in the presence of $MnCl_2$, the substrate D-xylose, D-xylose plus $MnCl_2$, and the inhibitor xylitol have been determined at 1.60, 1.60, 1.60, and 1.71 Å resolution, respectively. Both the cyclic and acyclic forms of D-xylose have been observed in these structures. After proposing a metal-mediated hydride shift mechanism, we compare this work to other crystallographic studies of xylose isomerase.

MATERIALS AND METHODS

The enzyme used in this study was prepared at Cetus Corp. using a strain of *E. coli* that expresses the gene for *Streptomyces rubiginosus* xylose isomerase (XI).[28] The enzyme was stored in the presence of 1.0 mM $MgCl_2$. Crystals were prepared using the hanging drop vapor diffusion technique.[29] An 8–9 mg/ml solution of enzyme in 17–25% saturated ammonium sulfate, 0.5 mM $MgCl_2$, 50 mM HEPES, pH 7.0 was equilibrated by vapor diffusion against 35–50% saturated ammonium sulfate also buffered with 50 mM HEPES at 4°C. Large crystals appeared within several days. These crystals are isomorphous with those described by Carrell et al.,[27] and belong to space group *I*222 with mean unit cell dimensions of $a = 93.6$ Å, $b = 99.2$ Å, and $c = 102.3$ Å and with one monomer per asymmetric unit.

The uranyl and platinum derivatives reported by Carrell et al.[27] were reproduced by soaking crystals in 2 mM $UO_2(NO_3)_2$ or $K_2Pt(SCN)_4$ buffered with 50% ammonium sulfate, 50 mM HEPES, pH 7.0. The enzyme was also cocrystallized with inhibitor (xylitol) or substrate (D-xylose) and/or $MnCl_2$. To the basic crystallization procedure described above the following were added: 50 mM xylitol, 40 mM D-xylose, 10 mM $MnCl_2$, and 50 mM $MnCl_2$ + 40 mM D-xylose (see Table I).

X-Ray diffraction data were collected using a Siemens (formerly Xentronics) electronic area detector mounted on a Supper oscillation camera controlled by a Cadmus 9000 microcomputer. During data collection the area detector chamber was mounted 10 cm from the crystal. The carriage angle (the angle between the normal to the detector face and the direct beam) was varied from 0° to 35°, enabling the detector to intercept data from ∞ to 1.58 Å, depending upon its position. Diffraction data collected by the area detector are recorded as a series of discrete frames or electronic images, each comprising a 0.20° or 0.25° oscillation counted for between 30 and 110 sec, depending upon the carriage angle. Usually 400 to 480 data frames, corresponding to 100° of crystal rotation about a vertical axis, were accumulated on a hard disk. Subsequently, the data were transferred by an Ethernet link to a Digital Equipment Corporation VAX 11/780 or a Silicon Graphics Personal Iris computer for processing. During the course of data collection, several data sets from different crystal orientations were recorded. The crystals were repositioned in the X-ray beam by adjustment of the goniometer arcs, the *x*, *y*, and *z* translations, and (in the xylitol, $MnCl_2$, D-xylose, and D-xylose plus $MnCl_2$ data sets) a goniostat φ motor set 45° from vertical.

The X-ray source used to generate CuK_α radiation was an Elliot GX-21 rotating anode, operating at 70 mA and 40 kV with a 0.3 × 3.0 mm focal spot and a 0.3 mm collimator. Monochromatization was provided by a Huber graphite monochromator. All data collection was performed at well-controlled room temperature (16–20°C). The crystals were very stable in the X-ray beam allowing collection of an extensively replicated data set to 1.60 Å from a single crystal. The XENGEN software package was used for data reduction.[30]

A single crystal soaked in $K_2Pt(SCN)_4$ and two

TABLE II. Overall Statistics for Data Processing*

Data set	D_{min}(Å)	D_2(Å)	$R_w(I)$	$R_u(I)$	No. of reflections		Completeness
					Observed	Unique	
Native	1.64	1.82	4.50	5.17	236,341	49,910	0.94
$K_2Pt(SCN)_4$	2.15	2.52	7.21	10.39	65,154	23,309	0.88
$UO_2(NO_3)_2$	2.15	2.25	7.81	9.37	67,618	19,314	0.72
$UO_2(NO_3)_2$	2.15	2.20	6.77	7.52	68,473	24,757	0.92
$MnCl_2$	1.60	1.66	5.93	4.29	365,651	63,639	0.99
Xylitol	1.71	1.70†	6.19	7.08	291,153	45,797	0.90
Xylose	1.58	1.76	5.59	4.48	257,891	53,789	0.82‡
Xylose + $MnCl_2$	1.53	1.58	5.82	4.43	379,659	70,624	0.98

*Definitions:

D_{min} = smallest D spacing for which reflections were measured.

D_2 = D spacing at which $\langle I/\sigma(I)\rangle = 2$.

$R_w(I) = \Sigma\,[(I - \langle I\rangle)\,/\,\sigma]^2 / \Sigma[I/\sigma]^2$.

$R_u(I) = \Sigma\,|I - \langle I\rangle| / \Sigma\, I$.

$$\text{Completeness} = \frac{\text{Number of unique reflections measured}}{\text{Number of unique reflections possible}} \text{ to the stated resolution limit.}$$

†Extrapolated.

‡Xylose data were 99% complete to 1.80 Å.

crystals soaked in $UO_2(NO_3)_2$ were used to collect 2.8 Å data sets; the two uranyl data sets were refined separately. Heavy atom parameters were refined and phases calculated using conventional MIR methods as embodied in the XTAL software package.[31] A computer graphics system and the model building program FRODO[32] were used for interpreting electron density maps. The initial maps were computed with phases obtained by combining computed and MIR phases with Fourier coefficients weighted by the figure of merit.[33] Model phases were used for reflections beyond 2.8 Å. Once a trial structure had been obtained, restrained parameters least-squares procedures[34] modified by Finzel[35] to incorporate the fast Fourier algorithms of Ten Eyck and Agarwal[36,37] were used to refine the structure and to extend the resolution; 102 cycles of refinement were performed interspersed with 7 model building sessions on the graphics equipment.

The XI–xylitol structure was refined from the refined coordinates of the multiple isomorphous replacement (MIR) structure. The position of the xylitol molecule in the structure was determined by examination of an $F_o - F_c$ difference electron density map using phases from the native structure and amplitudes obtained from the xylitol-inhibited crystal. After addition of the inhibitor and four graphics sessions to adjust the model, the enzyme–inhibitor complex was refined as described for the uninhibited enzyme (55 cycles). The XI-xylose structure was refined from the XI–xylitol coordinates. Thirty-six cycles of refinement were performed with five model building sessions. The XI–xylose–$MnCl_2$ structure was refined from the XI–xylose coordinates. Thirty-one cycles of refinement were performed with five model building sessions. After the metal ion analysis (see below) crystals were prepared with $MnCl_2$. Data to 1.60 Å were obtained for a single crystal. Initial phases for this model were taken from the XI–xylose–$MnCl_2$ coordinates. The initial model was subjected to 31 cycles of refinement and four model building sessions on the graphics equipment. After the refinement of the MIR structure, it was not necessary to change any of the backbone conformations; only alternative positions and water molecules were added. The XI–xylitol, XI–xylose, XI–xylose–$MnCl_2$, and XI–$MnCl_2$ structures of xylose isomerase reported here will be deposited in the Brookhaven Protein Data Bank.[38]

To determine the identity of the divalent cation in the original crystal preparation, 11 native crystals were dried on filter paper and then dissolved in 10 ml of deionized double distilled water. The protein concentration was calculated from absorbance at 280 nm using the calculated molar extinction coefficient of 42,789 (based on the six Trp and nine Tyr per monomer found in the sequence). The sample was analyzed for manganese (Mn) and cobalt (Co) using furnace atomic absorption and magnesium (Mg) using flame atomic absorption by H. K. Gudnason at Biospherics Inc.

RESULTS

Multiple Isomorphous Replacement Structure Solution and Refinement

Results of data acquisition and processing for the native and the three heavy atom derivative crystals are presented in Table II. The heavy atom sites found in the 2.8 Å multiple isomorphous replacement (MIR) analysis were similar to those found by Carrell et al.,[27] as shown in Table III. The final figure of merit for 11,246 reflections to 2.8 Å was 0.64.

The 2.8 Å MIR electron density map was very clear, enabling an unambiguous tracing of the polypeptide chain consistent with the 4.0 Å structure and a placement of nearly the entire amino acid se-

TABLE III. Heavy-Atom Refinement Results*

Compound	R_C	R_K	E/F_H	X	Y	Z	B	Occ†
$K_2Pt(SCN)_4$	0.569	0.178	0.809	0.247	0.321	0.286	20.86	0.883
				0.155	0.129	0.378	27.19	0.819
$UO_2(NO_3)_2$	0.464	0.106	0.409	0.141	0.348	0.421	13.26	1.000
				0.085	0.364	0.430	19.98	0.324
				0.287	0.146	0.397	67.99	0.231
				0.277	0.257	0.190	58.34	0.212
$UO_2(NO_3)_2$	0.517	0.110	0.438	0.141	0.348	0.421	11.84	0.888
				0.086	0.365	0.428	22.37	0.262
				0.286	0.145	0.399	66.31	0.136
				0.278	0.258	0.187	49.20	0.130

*Definitions:
$R_C = \Sigma| F_{PHobs} - F_P | - F_H | / \Sigma | F_{PHobs} - F_P |$.
$R_K = \Sigma| F_{PHobs} - F_{PHcal} | / \Sigma | F_{PHobs} |$.
$E/F_H = \Sigma| F_{PHobs} - F_{PHcal} | / \Sigma | F_H |$.
F_P = protein structure factor; F_H = heavy atom structure factor.
F_{PHobs} = observed heavy atom derivative structure factor.
F_{PHcal} = calculated heavy atom derivative structure factor.
Occ = fractional occupancy of site.
†The occupancies have been scaled such that the largest occupancy equals 1.00.

quence. The initial R was 46%, and the final R factor was 0.163 at 1.64 Å (see Table IV). Refinement and graphical rebuilding resulted in the determination of a model structure containing 385 residues (residues 1, 2, and 388 are not visible), 320 ordered water molecules, and 2 metal ions which we assumed were magnesium ions. When both metal ions were modeled as magnesium ions, a positive 4σ $F_o - F_c$ difference peak was located on the catalytic cation (residue #391). We tried modeling both metal ions as calcium ions and allowed both the occupancies and temperature factors of the metal ions to vary during refinement. The occupancy and temperature factor for the catalytic cation are, respectively, 16 electrons and 11.52 Å^2 and for the structural cation (residue #392), 14 electrons and 17.73 Å^2, for the MIR structure. Since only 0.5 mM $MgCl_2$ was explicitly included in the crystallization buffers, it seems most reasonable that the protein had retained a divalent metal ion from the fermentation, most likely manganese for which it has the highest affinity ($K_d = 2.7 \times 10^{-5}$ M).[39] In the final model the catalytic cation was modeled as a partially occupied manganese ion and the structural cation as a fully occupied magnesium ion. This is not to say that the catalytic cation is partially occupied, we believe it to be fully occupied with a mixture of a magnesium ion and a manganese ion. We have chosen to call the two cations catalytic and structural to distinguish them; the reasons will be discussed later.

Overall Structure

The tetrameric enzyme is composed of subunits that exhibit the eight-helical–eight-stranded parallel β-barrel which is a common motif found in several other enzymes.[40–42] Residues 3–317 form the eight-helical–eight-stranded β-barrel while the C-terminal residues 318–387 depart from the main globular domains to form an extended tail composed of partially helical segments.[27] The α/β barrel is very distorted,[43] so it was not possible to assign which set of strands (odd or even) contribute side chains to the center layer of interior residues of the barrel, according to the simple pattern described by Lesk.[44] A pair of monomers form a tightly coupled dimer by extensive contacts of the core of the first monomer interacting with the C-terminal tail of the second, and the core of the second interacting with the C-terminal tail of the first. There are 44 hydrogen bonds involved in this "tight" dimer interaction (Fig. 2A). A pair of these dimers then associates to form the active tetramer. Only 12 hydrogen bonds are involved in this "weaker" dimer–dimer interaction, of which 3 are unique. The overall structure of the monomer, dimers, and tetramers is best described as a dimer of dimers.[27] The *Streptomyces olivochromogenes* at 3.0 Å[45] and *Arthrobacter* at 2.5 Å[46] xylose isomerase structures have similar tetrameric architectures. An assignment of the α-helix and β-sheet secondary structure elements is presented in Table V.

The active site of xylose isomerase is located at the C-terminus of the β-barrel and is situated close to the crystallographic 2-fold axis (the crystalline y axis at $x = 0$, $z = 1/2$, which relates the two weakly interacting dimers, see Fig. 2B). The active site opening is filled with ordered solvent molecules although the entrance to the pocket is lined with hydrophobic side chains. Phe-26 from the neighboring weak dimer extends into the active site. In addition to the Phe-26 from the neighboring molecule, residues Phe-94, Trp-16, and Trp-20 line one side of the active site pocket. The active site can be described as an amphipathic pocket, with hydrophobic residues

TABLE IV. Summary of Crystallographic Refinement

	Resolution (Å)	No. of reflections			RMS deviation final model†			
		Measured	Used ($I>2\sigma$)	R factor*	Bonds	Angles	1 4	ω Planarity‡
MIR	1.64	49,910	43,130	0.163	0.020	0.032	0.040	3.9
$MnCl_2$	1.60	63,639	55,577	0.141	0.022	0.032	0.045	4.7
Xylitol	1.71	45,797	39,229	0.149	0.020	0.031	0.041	4.6
Xylose	1.60	53,789	43,624	0.151	0.022	0.032	0.044	4.6
Xylose + $MnCl_2$	1.60	70,624	58,447	0.135	0.020	0.031	0.045	4.6

*R factor = $\Sigma|F_o-F_c| / \Sigma F_o$.
†The RMS deviation in Å of the final model represents the root mean squared differences between observed values and the target values obtained from peptide powder diffraction studies.
‡The RMS deviation in degrees of the final model's peptide torsion angles from 180° or 0°

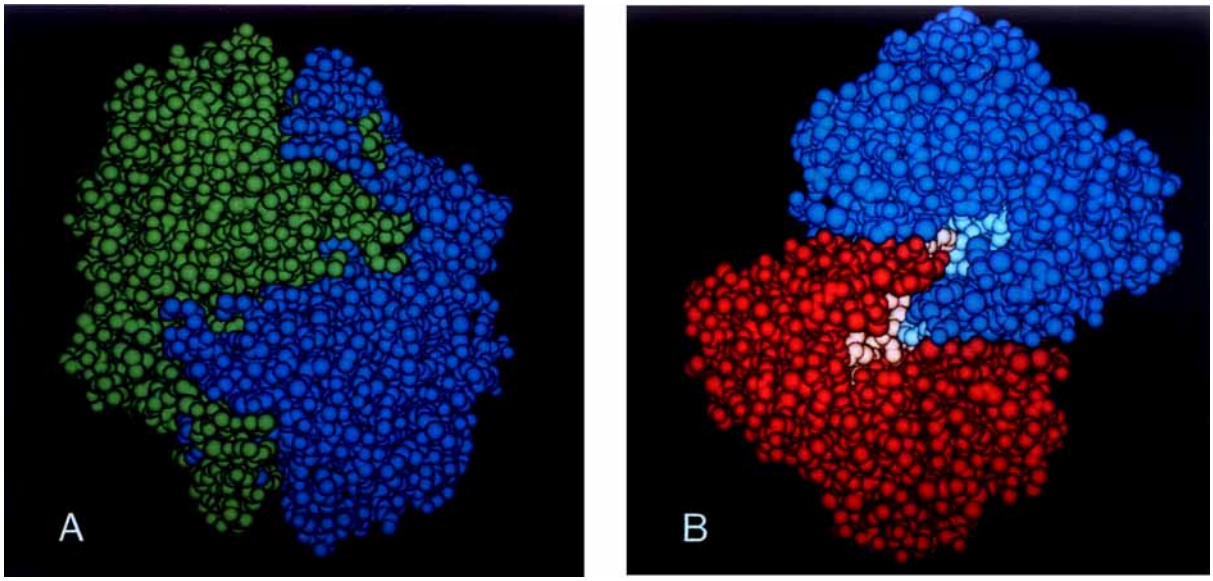

Fig. 2. Surface diagrams of the xylose isomerase dimers. **A:** "Tight" dimer, looking down the crystallographic two-fold axis around x at y = 1/2, z = 1/2. **B:** Weak dimer, looking down the crystallographic two-fold axis around y at x = 0, z = 1/2. The two active sites are high-lighted.

lining one side and hydrophilic residues the other. The hydrophilic residues are involved in either the binding of the two divalent cations found in the active site, and/or the binding and catalysis of the substrate.

Metal Ion Binding Sites

The metal-ion analysis showed the native crystals contained 0.6 equivalents, less than 0.6 equivalents and less than 0.1 equivalents per monomer of Mn, Mg, and Co, respectively. These results were obtained at the limits of the instrument's sensitivity. Due to the ambiguity of these results and the occupancies at metal sites in the MIR structure, we prepared a crystal with $MnCl_2$, since the protein has the highest affinity for manganese ($K_d = 2.7 \times 10^{-5}$ M).[39]

The $MnCl_2$ structure was refined from the XI–xylose–$MnCl_2$ coordinates without the sugar. The final refined model for the $MnCl_2$ structure contains 386 residues (residue 1 and 388 again are not visible), 409 ordered water molecules (89 more than in the MIR structure), and 2 manganese ions. Alternate conformations were found for the side chains of Arg-23, Arg-66, Arg-76, Lys-85, Glu-132, Met-158, Arg-205, Lys-253, Arg-266, Lys-289, Glu-328, Arg-340, Val-362, and Arg-387 and all of residue Asp-175. A Ramachandran plot (ϕ–ψ map) shows only one nonglycine residue with abnormal values, Glu-186 (see Fig. 3). The peptide bond between Glu-186 and Pro-187 is in the *cis* conformation.[43] Figure 4 shows the variation of B along the polypeptide chain. The final occupancies and temperature factors for the catalytic Mn^{2+} (391) are, respectively, 23 electrons and 11.0 Å^2 and for the structural Mn^{2+} (392), 18 electrons and 10.8 Å^2.

The coordination geometry for both manganese ions is best described as 6-coordinate octahedral, al-

TABLE V. Secondary Structure Elements of Xylose Isomerase

β-Strand	α-Helix
11–14	
	34–44
48–52	
	63–80
86–88	
	107–127
131–134	
142–143	
	152–172
175–178	
188–189	
	194–201
210–212	
	216–220
	226–235
245–246	
	263–275
282–285	
	294–320
	322–330
	345–350
	361–365
	370–382

though the coordination geometry for the catalytic magnesium (391) in the MIR structure is 5-coordinate. The structural manganese ion has four protein ligands: Glu-181, Glu-217, Asp-245, and Asp-287 and two ligated water molecules. The catalytic manganese ion (391) has five protein ligands: Glu-217, His-220, Asp-255 (both OD1 and OD2), and Asp-257, and one water molecule ligand. Both of these manganese ions have a mean ligand coordination distance of 2.26 Å (see Table VI). The manganese ions are 4.9 Å apart and share a common ligand, Glu-217 (see Fig. 5). A similar situation is found in concanavalin A, where the manganese and calcium binding sites are 4.25 Å apart and share the common ligands Asp-10 and Asp-19.[47] The six acidic groups coordinated to the two metals are hydrogen bonded to neighboring neutral amino acids such as Asn and His. Six basic groups are found in the active site, two lysine and four histidines; only the two lysines would be charged at the catalytically optimum pH of 8.5. Lys-183 is hydrogen bonded to a water molecule coordinated to the catalytic Mn^{2+}. Both divalent cations are involved in the binding of the competitive inhibitor xylitol and the extended form of the substrate D-xylose.

Xylose Isomerase–Xylitol Structure

The first difference map in the XI–xylitol refinement clearly showed the xylitol in an extended conformation (see Fig. 6A). Five water molecules are displaced from the active site when xylitol binds. These water molecules in the native structure occupy approximately the same positions as do the oxygen atoms in xylitol bound to the enzyme. The O2 and O4 hydroxyls are coordinated directly to the structural magnesium ion, and the O1 hydroxyl is coordinated directly to the catalytic magnesium ion (see Fig. 7A). The coordination geometry around the structural magnesium ion is unchanged from the $MnCl_2$ structure, remaining octahedral and having a mean coordination distance of 2.17 Å (see Table VI). In contrast, the geometry around the catalytic magnesium ion has changed considerably. Upon binding xylitol, this Mg^{2+} ion now has seven ligands instead of six, the mean coordination distance has increased to 2.77 Å, and the Mg^{2+} has a high temperature factor of 41.5 $Å^2$, compared to 10.4 $Å^2$ for the structural Mg^{2+}. We believe that these differences are principally a result of xylitol binding and do not reflect the difference between manganese and magnesium ions. Unlike the XI–xylose–$MnCl_2$ structure (see below) only one position is found for the catalytic Mg^{2+}. Three hydrogen bonds are made to the xylitol from the enzyme: NZ of Lys-183 to O1; OD2 of Asp-287 to O3; and NE2 of His-54 to O5 (see Fig. 8 and Table VII). The Lys-183 and the catalytic Mg^{2+} position the O1 of xylitol such that its O1–O2 diol is in a *cis* conformation with a O1–Cl–C2–O2 torsion angle of −3°. The present crystallographic results differ significantly from early conclusions based on NMR data,[48] where the distance between inhibitor and manganese ions was estimated to be 9 Å and it was concluded that protein and/or water intervenes between the substrate and metal ions.

Changes in the protein structure due to inhibitor binding are confined to the active site region. A comparison of the native and xylitol inhibited enzyme structures is shown in Figure 9C. The most notable changes are the positions of the metal ions and ligands interacting with them. The catalytic cation (391) moves 1.0 Å in a direction closer to the inhibitor presumably to promote interaction with the xylitol while the structural cation (392) shifts only 0.4 Å. Ligands undergoing the largest change are Asp-255, Glu-217, Asp-287, and His-220 (Fig. 9C). Asp-255 has an alternative conformation (see Fig. 10A). The maximum shifts in a carboxylate atom in Asp-255, Asp-287, and Glu-217 are 1.00, 0.85, and 0.73 Å, respectively, and 0.65 Å for the imidazole ring of His-220.

Xylose Isomerase–Xylose–$MnCl_2$ Structure

When we first examined the maps of XI–xylose–$MnCl_2$ (40 mM D-xylose and 50 mM $MnCl_2$), we reexamined the crystal preparation to make sure the crystal had been taken from a D-xylose cocrystallization rather than a xylitol cocrystallization, since the F_o-F_c difference map of XI–xylose is very similar to the XI–xylitol map (see Fig. 6B). Upon refinement of the XI–xylose–$MnCl_2$ structure, however, a number of differences became apparent. The chiral

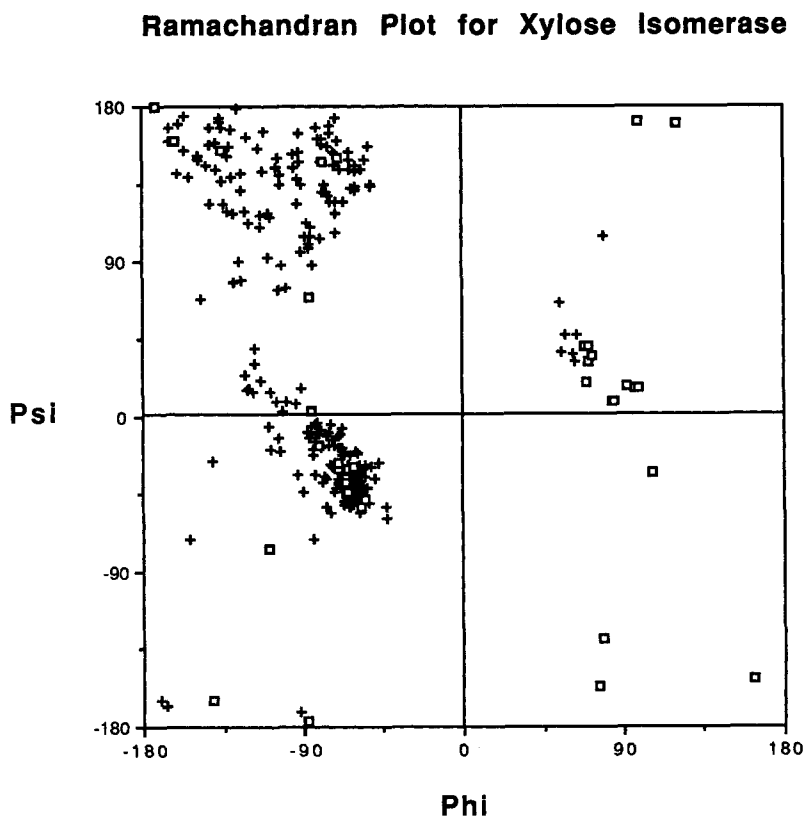

Fig. 3. Ramachandran plot for xylose isomerase. (□) Glycyl residues; (+) other residues.

center at C2 was initially restrained to be chiral (as it would be in D-xylose), but it was clear from the electron density and the refinement that C2 "wanted" to be planar (see Fig. 7B). Neither chiral nor planar restraints were applied in the final refinement. The product D-xylulose has a planar C2; thus this structure may be better described as a XI–xylulose structure. This suggests that the extended D-xylulose enzyme complex is more stable than the extended D-xylose enzyme complex, even though at equilibrium the ratio of D-xylulose to D-xylose is 0.20 to 0.80.[16] Unlike the XI–xylitol structure, Asp-255 in the XI–xylose–$MnCl_2$ structure did not have an alternative position (see Fig. 10B). Like the XI–xylitol structure the O1–C1–C2–O2 torsion was in a *cis* conformation, with a torsion angle of 3°. In addition to the extended form of the xylulose, there is density suggestive of the cyclic form of xylose, discussed below. The cyclic and extended forms have been modeled with occupancies of 0.2 and 0.8, respectively, and have mean *B*s of 25.4 and 12.4 Å^2, respectively. These occupancies were manually adjusted, until no interpretable difference peaks were found. We estimate that these occupancies are accurate to ±0.1.

Unlike the XI–xylitol structure, the XI–xylose–$MnCl_2$ structure shows two positions for the catalytic Mn^{2+}. The high occupancy position, with an occupancy of 0.98 (23 electrons) and a *B* of 10.1 Å^2, is octahedrally coordinated with a mean coordination distance of 2.28 Å (see Table VI), and is not coordinated to the sugar (see Fig. 7B). A water molecule that is coordinated to the high occupancy Mn^{2+} position is hydrogen bonded to the O1 and O2 of the D-xylulose (Table VII), and to OD1 of Asp-257 (2.60 Å). We will propose that Asp-257 removes a proton from this water and the resulting hydroxide ion is involved in transferring a proton from the O2 of D-xylose to the O1 of D-xylulose during the isomerization reaction. The second Mn^{2+} position is 1.76 Å from the high occupancy Mn^{2+} site and 1.92 Å from the aforementioned water molecule, and has an occupancy of 0.18 (four electrons) and a *B* of 10.2 Å^2. Thus, the alternative position of the Mn^{2+} coordinates to the O1 and O2 of xylulose, displacing the water molecule. We were unable to locate an alternate position for this water molecule, but if its occupancy is also around 0.2 (1.6 electrons) we would be able to distinguish it from noise in the electron density. The alternative position for this water molecule is most likely still hydrogen bonded to Asp-257 and coordinated to the catalytic Mn^{2+}. We will propose that the low occupancy catalytic Mn^{2+} position stabilizes an oxyanion after a proton has been removed from the O1 or O2 of the substrate by the hydroxide ion. The low occupancy Mn^{2+} site is also

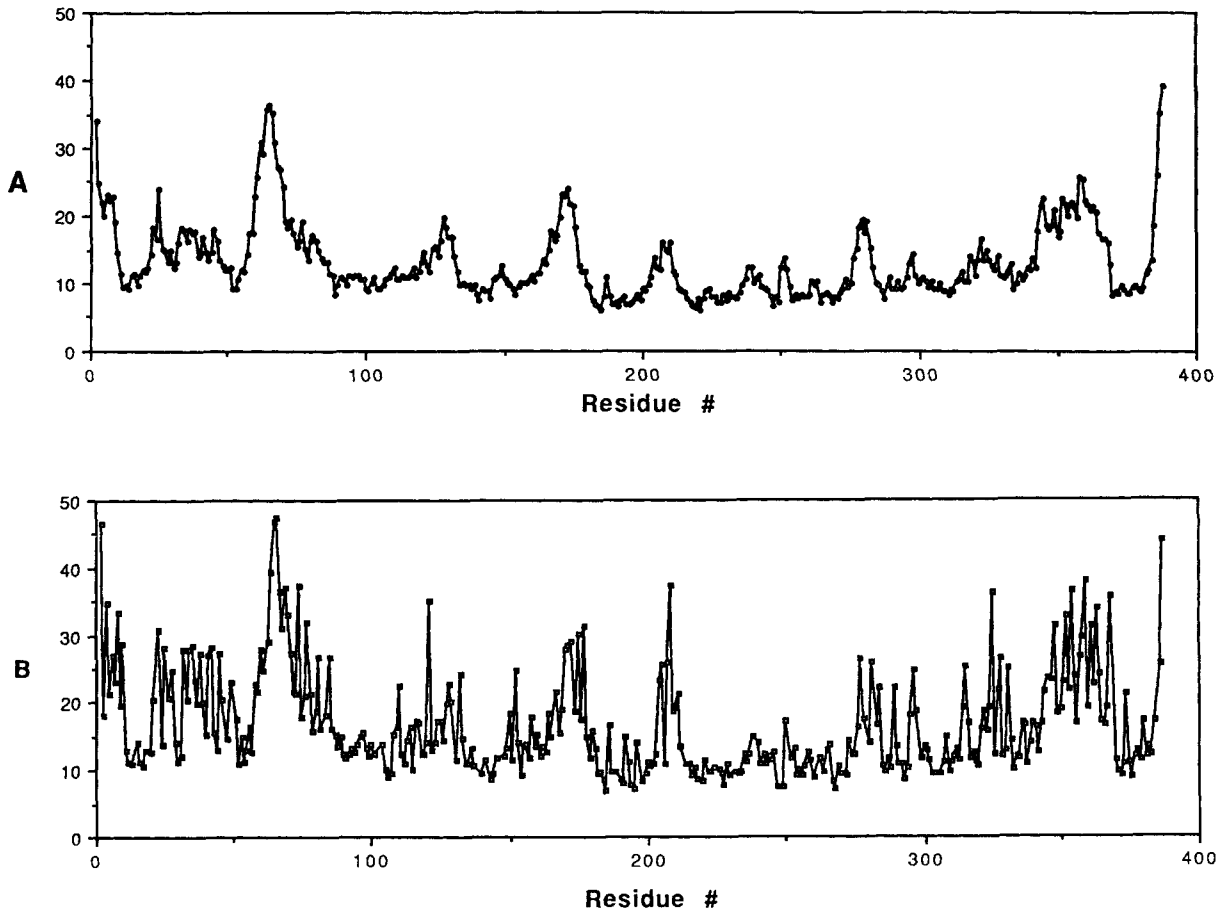

Fig. 4. Variation in *B* along the polypeptide chain. No *B* factor is shown for residue 1 because it was not seen in the electron density map. (**A**) Backbone atoms (N, C_α, C, and O); (**B**) Side chain atoms.

TABLE VI. Ligands Coordinating the Two Active Site Metal Ions

Structure	$MnCl_2$		Xylitol Mg^{2+}		Xylose + $MnCl_2$	
Metal ion	Ligand	Distance (Å)	Ligand	Distance (Å)	Ligand	Site 1 Distance (Å)	Site 2 Distance (Å)
Catalytic 391*	OE1 Glu-217	2.11		3.08		2.12	2.71
	OE2 Glu-217						2.51
	NE2 His-220	2.32		2.79		2.43	2.09
	OD1 Asp-255	2.34		2.49		2.28	(3.11)†
	OD2 Asp-255	2.29		2.22		2.29	
	OD2 Asp-257	2.24		2.85		2.30	(3.72)
	Water	2.23		3.10		2.23	(1.92)
		Mean = 2.26	O1 xylitol	2.84	O1 xylose		2.61
				Mean = 2.77	O2 xylose		2.35
						Mean = 2.28	Mean = 2.45
Structural 392	OE1 Glu-181	2.09		2.03		2.14	
	OE2 Glu-217	2.12		2.06		2.17	
	OD1 Asp-245	2.18		2.30		2.18	
	OD2 Asp-287	2.15		2.21		2.19	
	Water	2.42	O2 xylitol	2.19	O2 xylose	2.31	
	Water	2.62	O4 xylitol	2.22	O4 xylose	2.34	
		Mean = 2.26		Mean = 2.17		Mean = 2.22	

*The catalytic and structural divalent cations are arbitrarily numbered 391 and 392, respectively.
†The values in parentheses were not used in the calculated mean distance.

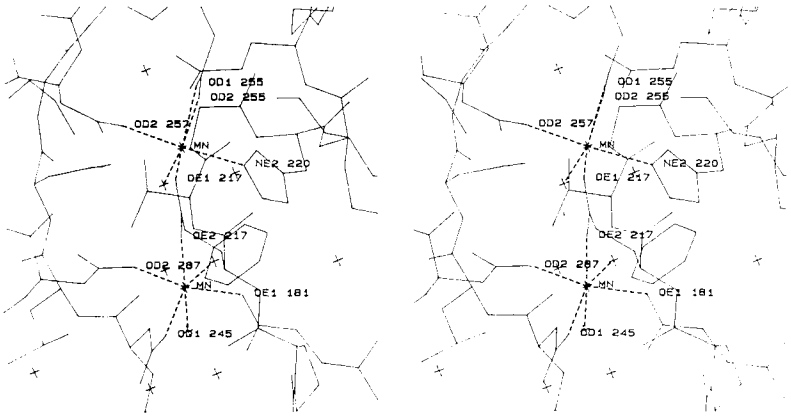

Fig. 5. Manganese ions at the active site of xylose isomerase without substrate bound in the $MnCl_2$ structure. Dashed lines highlight the metal coordination. The catalytic Mn^{2+} is above the structural Mn^{2+}.

octahedrally coordinated, but with a nonoptimal mean coordination distance of 2.45 Å.

Xylose Isomerase–Xylose Structure

The final structure we will examine is a structure in which xylose isomerase was cocrystallized with xylose, without additional $MnCl_2$ present (XI–xylose structure). The electron density of this structure clearly showed a cyclic sugar bound to the enzyme (see Fig. 6C). The fit to the electron density is not good for either a cyclic xylose or cyclic xylulose, but a six-membered ring of α-D-xylose fits better than a five-membered ring of D-xylulose. In addition, density can be found for an extended form of the sugar, and this has also been modeled. The cyclic and extended forms have been modeled with occupancies of 0.3 and 0.4, respectively, and have mean *B*s of 22.8 and 25.8 Å^2, respectively. As in the XI–xylose–$MnCl_2$ structure, we estimate that these occupancies are accurate to ±0.1. Both the structural and catalytic magnesium ions have low occupancies, 0.27 and 0.47, respectively. The structural magnesium ion has close contacts with the O3 and O4 hydroxyls of the cyclic xylose, suggesting that it is displaced when the cyclic xylose is bound. The binding of the cyclic xylose is very similar to other sugar-protein binding interactions.[49,50] The O2, O3, and O4 hydroxyls show cooperative hydrogen bonding with Glu-181 and Asp-287, and the sugar has hydrophobic interactions with Trp-16 (see Fig. 11 and Table VIII). We had originally thought that the preference that xylose isomerase displays for α-D-xylose and α-D-glucose is due to the steric hindrance that would occur between the β-O1 hydroxyls of these sugars and Trp-137 and Phe-94.[51] We now believe that the preference is due to the inability of the enzyme to perform the ring opening reaction on the β-D substrates, as suggested by Collyer et al.[52]

The NE2 of His-54 is within hydrogen bonding distance of the ring oxygen (2.99 Å) and the O1 hydroxyl (3.30 Å) of the cyclic α-D-xylose (see Fig. 11B and Table VIII). In addition the ND1 of His-54 is hydrogen bonded to the OD1 of Asp 57. This suggests that His-54 and Asp-57 are involved in catalyzing the sugar ring opening step in the xylose isomerase mechanism. A similar structure has been reported by Farber et al.,[53] for the *Streptomyces olivochromogenes* enzyme, in which they first suggested the catalytic role for these conserved residues. There are four water molecules within 4.5 Å of the imidayole ring of His-54. If His-54 is involved in forming an enediol intermediate as suggested by Carrell et al.,[25] these water molecules would exchange with the extracted proton.

DISCUSSION

Chemical Conversion of D-Xylose to D-Xylulose

The chemical conversion of D-xylose to D-xylulose or of D-glucose to D-fructose is a subset of the Lobry de Bruyn–Alberda van Ekenstein transformation reaction.[7–9] Wohl and Neuberg[10] first proposed that the aldose–ketose isomerization proceeds through an enediol intermediate. These transformations can be either acid or base catalyzed.

When D-glucose is incubated in the presence of $Ca(OD)_2$ (deuterated calcium hydroxide) for 10–20 min at room temperature the initial products formed are D-glucose with deuterium replacing the hydrogen bound to C-1 and fructose with deuterium replacing one of the two C-1 hydrogens.[11] If the reaction is allowed to go to equilibrium, then both hydrogens on C-1 of fructose become deuterated.[54] At equilibrium the final mixture of sugars is 66.5% D-glucose, 28.6% D-fructose, and a trace of D-mannose (0.8%). These results are consistent with a *trans*-enediol intermediate between D-glucose and D-fructose and a *cis*-enediol intermediate between D-

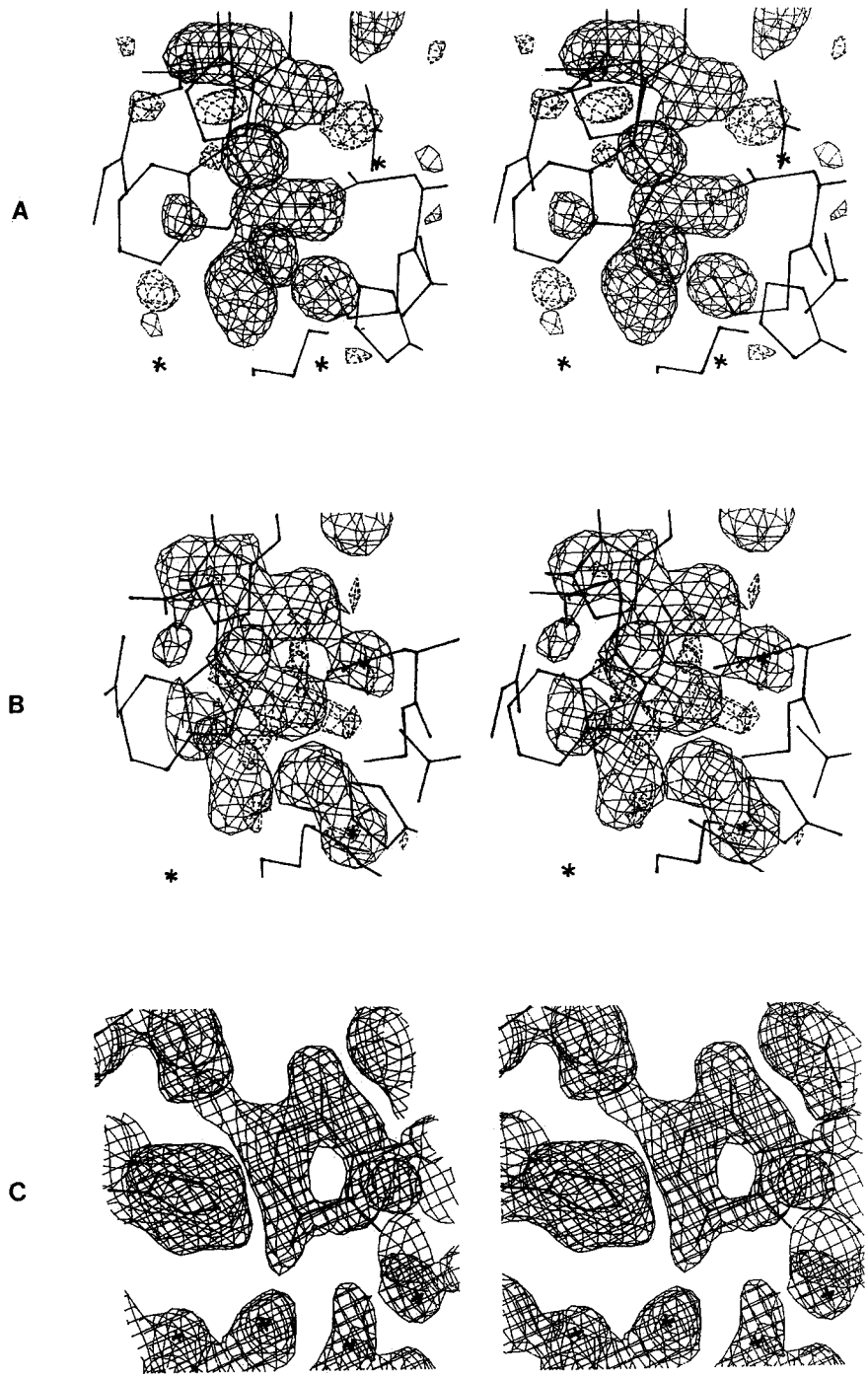

Fig. 6. (**A**) First F_o-F_c difference map of XI–xylitol structure, contoured at 3σ. (**B**) First F_o-F_c difference map for the XI–xylose–$MnCl_2$ structure, contoured at 3σ. (**C**) Final $2F_o-F_c$ map for the XI–xylose structure, showing the cyclic α-D-xylose, contoured at 0.55σ (4σ in the F_o-F_c map).

fructose and D-mannose. Studies of the base-catalyzed transformation of D-arabinose to D-ribose have shown a lack of exchange with solvent,[12] suggesting a hydride transfer is occurring and that enolization is not an obligatory first step in this rearrangement.

The acid-catalyzed transformations between D-glucose and D-fructose[13] and between D-xylose and D-xylulose[14] do not show hydrogen exchange with the solvent as do the base-catalyzed transformations. Since an enediol intermediate would exchange with the solvent, Ramchander and Feather[14] proposed a hydride shift or conducted tour mechanism

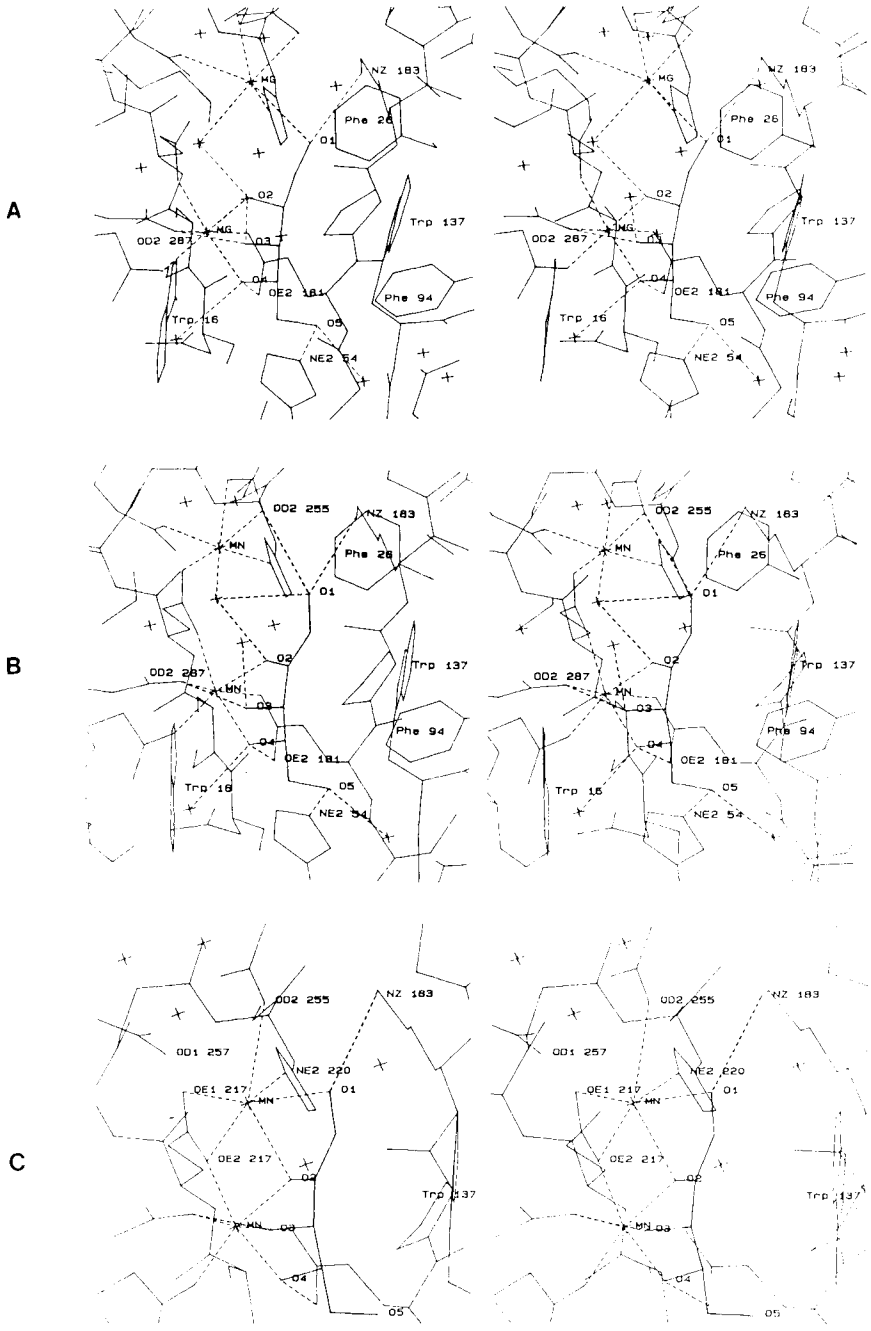

Fig. 7. (**A**) Xylitol bound in the Xl–xylitol structure. (**B**) Extended D-xylose bound in the Xl–xylose–$MnCl_2$ structure, showing the high occupancy catalytic Mn^{2+} site. (**C**) Extended D-xylose bound in the Xl–xylose–$MnCl_2$ structure, showing the low occupancy catalytic Mn^{2+} site, without the catalytic water molecule. Dashed lines highlight possible hydrogen bonds and manganese ion coordination.

in which the proton remains associated with the developing π-electron cloud, and could be stabilized by a negative charge. This lack of hydrogen exchange with solvent upon the isomerization is also observed for the enzymatic reaction.

Xylose Isomerase Biochemistry

Xylose isomerase has been shown to transfer a proton from the 2-position of D-xylose (or D-glucose) to the 1-pro-R position of D-xylulose (or D-fructose). Schray and Rose[17] explain this by suggesting that if the proton is removed and replaced by a single base in forming an enediol intermediate, this could be accomplished with the least amount of reorientation of the C1 and C2 hydroxyls through a *cis*-enediol (where the O1–C1–C2–O2 torsion angle is planar and in the *cis* conformation; see scheme I in Schray and Rose[17]). A *trans*-enediol intermediate would

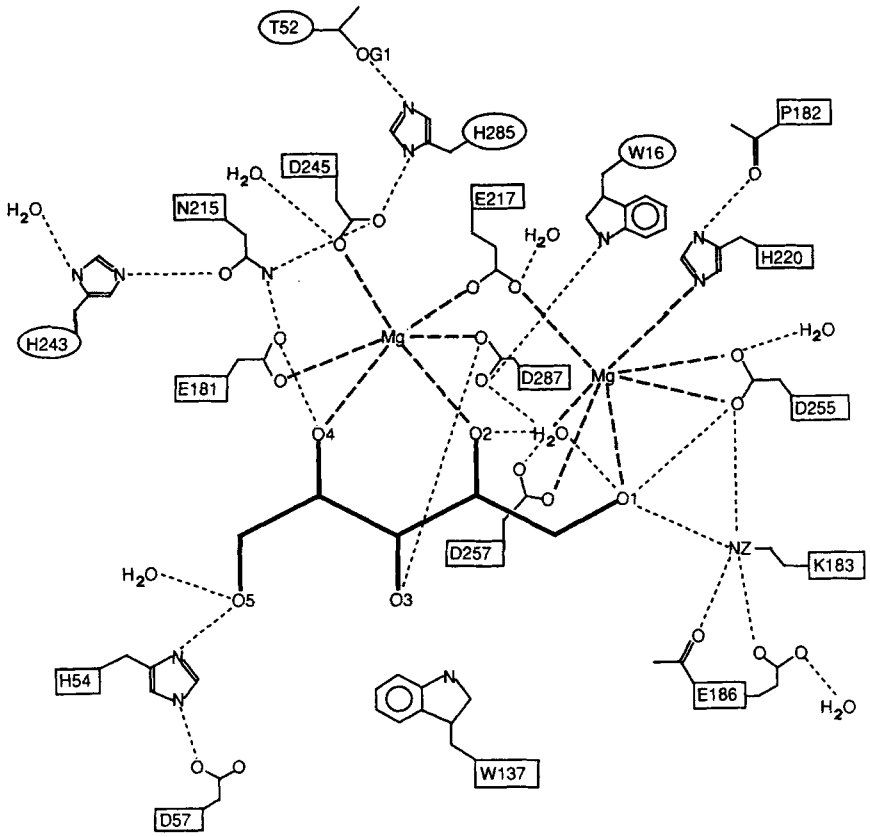

Fig. 8. Schematic diagram of the XI–xylitol structure. The metal coordination is shown in bold dashed lines and the hydrogen bonds are shown as light dashed lines. The conserved residues have boxes around the number, whereas the unconserved residues have ellipses.

TABLE VII. Probable Hydrogen Bonds Between Xylitol and Extended Xylose and Neighboring Protein Groups of Water Molecules

		Distance (Å)	
Substrate	Protein	Xylitol	Xylose
O1	NZ Lys-183	2.96	3.06
O1	Water		3.12
O2	Water	2.97	2.97
O3	OD2 Asp-287	2.81	2.91
O3	Water	3.04	3.20
O4	OE2 Glu-181	2.47	2.59
O4	Water	3.02	2.97
O5	NE2 His-54	2.87	2.87
O5	Water	2.64	2.63

TABLE VIII. Probable Hydrogen Bonds Cyclic α-D-Xylose and Neighboring Protein Groups or Water Molecules

α-D-Xylose	Protein	Distance (Å)
O	NE2 His-54	2.99
OH1	NE2 His-54	3.30
OH1	Water	2.57
OH2	OD2 Asp-287	3.01
OH2	Water	2.50
OH2	Water	3.18
OH2	Water	3.17
OH3	OD2 Asp-287	2.42
OH3	OE1 Glu-181	2.46
OH3	Water	3.14
OH4	OE2 Glu-181	2.74
OH4	Water	2.65

produce D-lyxose (or D-mannose) from D-xylose (or D-glucose). Furthermore, the proton transferred is not exchanged with solvent,[15,16] suggesting a hydride shift mechanism. In a hydride shift mechanism the conformation around the O1–C1–C2–O2 torsion angle also must have a *cis* conformation for the same reasons. We have shown that both xylitol in the XI–xylitol structure and the extended D-xylulose in the XI–xylose–$MnCl_2$ structure have a cis conformation.

The catalytic pH optimum of most xylose isomerase enzymes is around 8.5. The enzyme becomes active with the deprotonation of a group with a pK_a of 6.5 and protonation of a group with a pK_a of 9.5.[19] Furthermore, both histidine and lysine have been implicated in the catalytic mechanism by chemical modification.[20] Thus, one might expect to see a protonated lysine and a neutral histidine in-

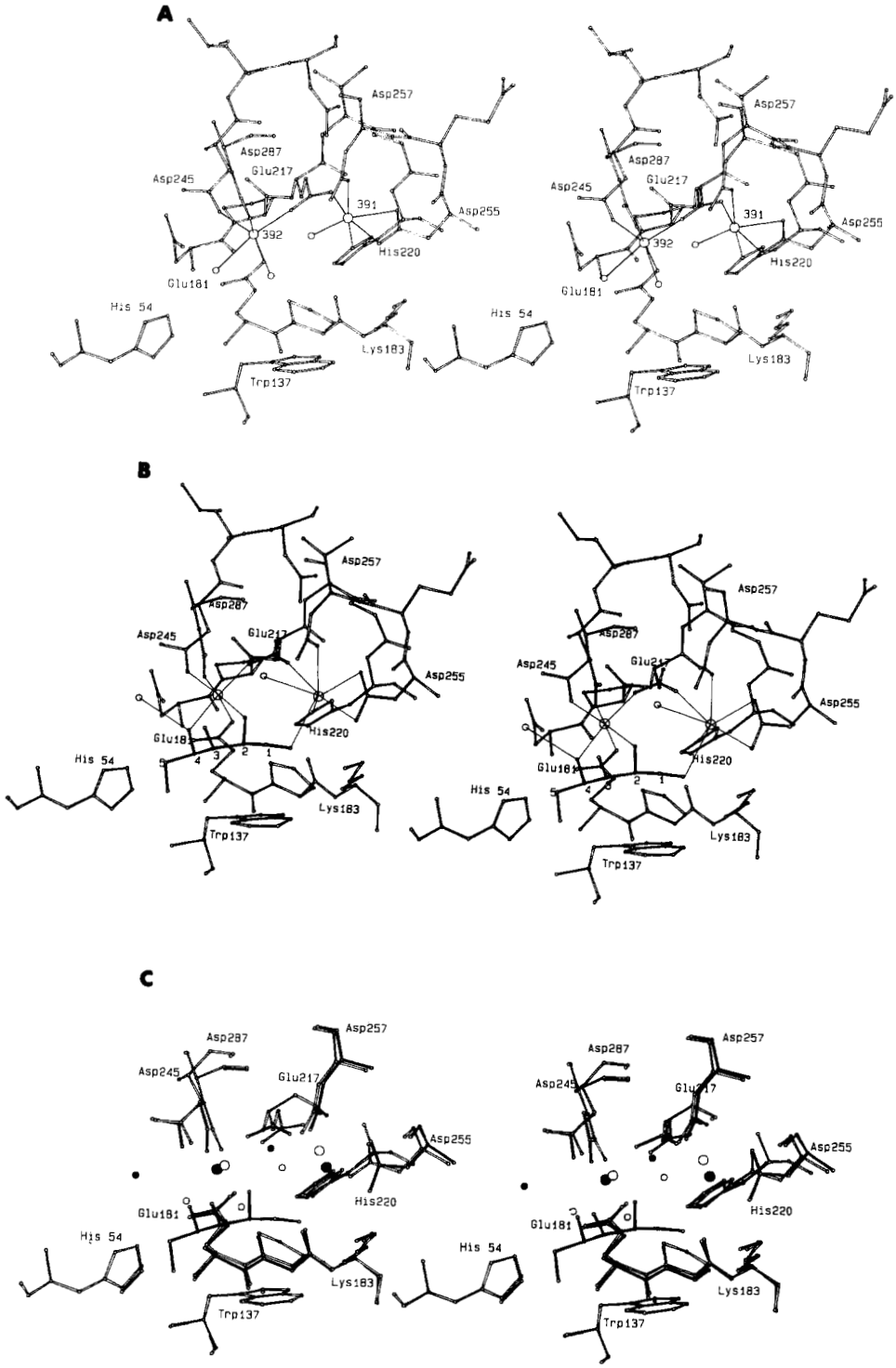

Fig. 9. Stereo models of the active site region. Thin lines depict ligand–metal interactions. The large spheres represent the manganese ions and the smaller spheres, ordered solvent molecules. (**A**) The $MnCl_2$ structure with the manganese ions labeled 391 and 392; (**B**) XI–xylitol structure with each of the xylitol carbon atoms labeled; and (**C**) comparison of the $MnCl_2$ and XI–xylitol structures. The XI–xylitol structure is highlighted with solid bonds. Those metal ions and water molecules belonging to the XI–xylitol structure are indicated by the darkened spheres.

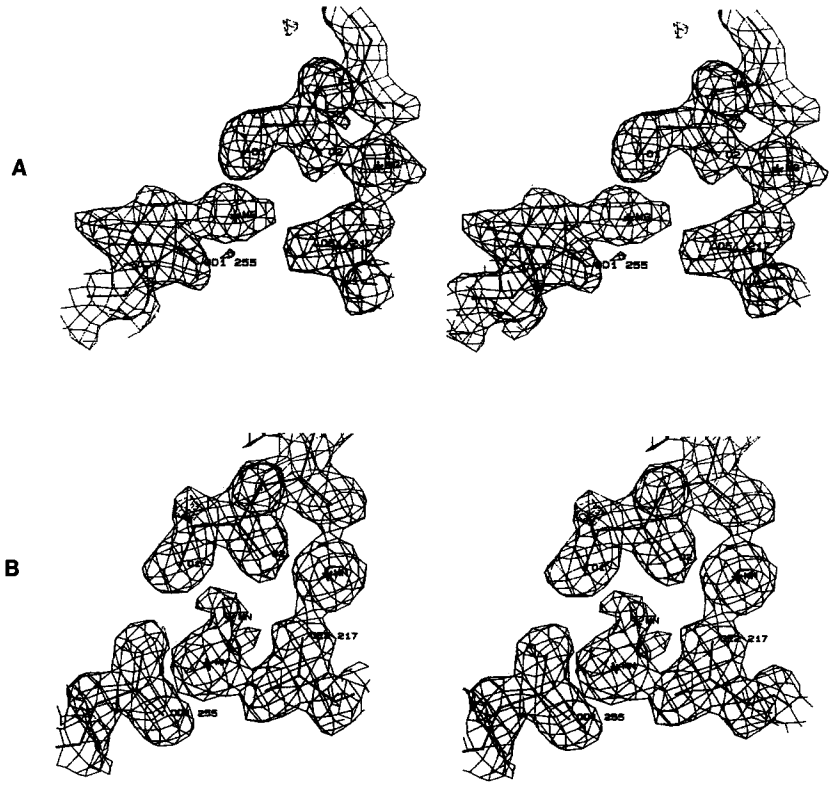

Fig. 10. (**A**) Final $2F_o-F_c$ map for the XI–xylitol structure, contoured at 0.75σ (5σ in the F_o-F_c map). (**B**) Final $2F_o-F_c$ (solid lines) and F_o-F_c (dashed lines) maps for the XI–xylose-$MnCl_2$ structure, contoured at 0.75σ (6σ in the F_o-F_c map) and 4σ for the $2F_o-F_c$ and F_o-F_c maps, respectively.

volved in the binding and catalysis. The structures show that both of these residues are involved in the binding of D-xylose and xylitol by xylose isomerase. His-54 is involved in the binding of cyclic α-D-xylose and Lys-183 is involved in the binding of the extended D-xylulose and the inhibitor xylitol.

The conversion of D-xylose to D-xylulose and of D-glucose to D-fructose by xylose isomerase is metal ion dependent. Mg^{2+}, Co^{2+}, and Mn^{2+} activate the enzyme, whereas Ni^{2+}, Ca^{2+}, Ba^{2+}, Zn^{2+}, Cu^{2+}, and Hg^{2+} do not.[19,21] The enzyme has no activity when dialyzed against EDTA for 24 hr.[19,22] The activity of the enzyme depends on the source of the enzyme, the divalent cation used, and the reaction one is interested in. The highest relative reactivities for the *Bacillus coagulans* enzyme were obtained with Mn^{2+} for D-xylose and with Co^{2+} for D-glucose,[21] whereas the highest relative reactivities for the *Streptomyces violaceoruber* enzyme were obtained with Mg^{2+}.[19] By Scatchard analysis the *Streptomyces violaceoruber* enzyme was shown to bind 8 Co^{2+} per tetramer or two Co^{2+} per monomer.[22,24] Callens et al.[23] showed that the *Streptomyces violaceoruber* enzyme has less than 10% of its maximum activity with one equivalent of Co^{2+} per monomer and has over 75% of its activity with two equivalents of Co^{2+} per monomer. From the present work it is clear that both divalent cations are directly involved in the binding of D-xylulose and xylitol.

The stability of the enzyme also depends on the amount and type of divalent metal ion present. Callens et al.[23] showed that the addition of one equivalent of Co^{2+} enhanced the structural stability of the *Streptomyces violaceoruber* enzyme, while the second equivalent is needed for activity. Co^{2+} is superior to Mg^{2+} in protecting the enzyme against thermal denaturation.[22,23] The first Co^{2+} appears to have a six-coordinate octahedral geometry, whereas the geometry of the second Co^{2+} is less evident, being four- or five-coordinate for the *Streptomyces violaceoruber* enzyme in the absence of substrate.[24]

Both divalent cations are needed for catalysis, but we have chosen to distinguish them by calling one catalytic and the other structural. We have chosen to call the catalytic cation "catalytic" for two reasons. First, it is the cation that is closest to the C1 and C2 of D-xylose or D-xylulose in our structures. Second, the catalytic cation shows more variations in its geometry than does the structural cation (see Table VI). The latter cation in our structures has a relatively invariant octahedral geometry, so we have chosen to call it the "structural" cation. We have assumed here that the Co^{2+} sites that Callens

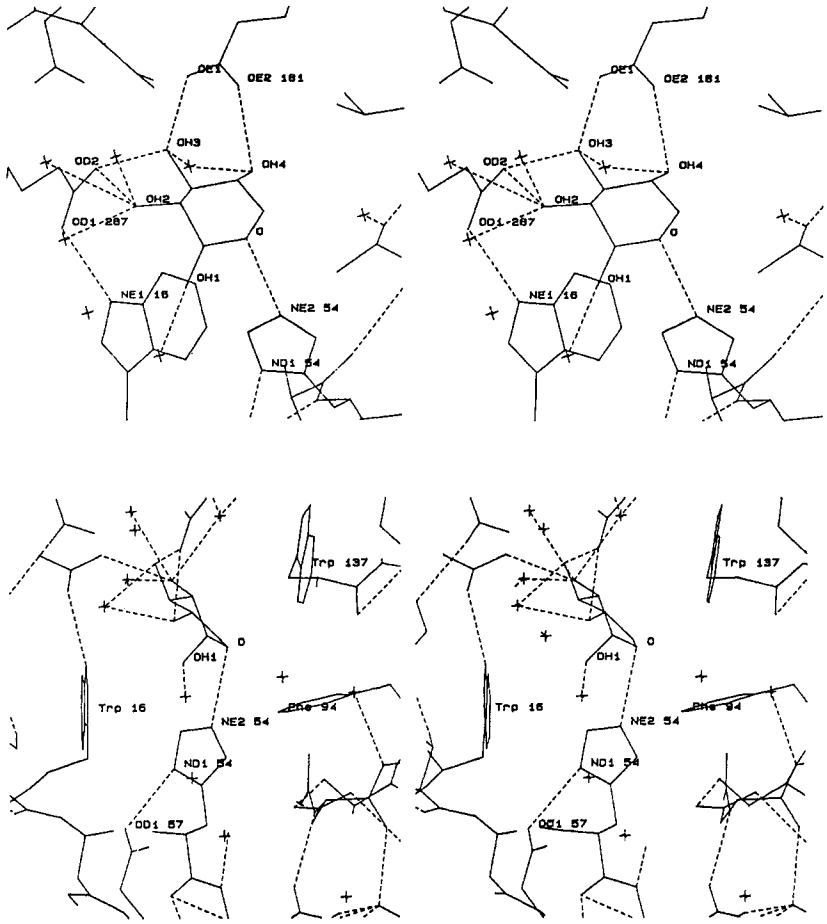

Fig. 11. Two views of the cyclic α-D-xylose bound to xylose isomerase in the XI–xylose structure. Phe-94, Trp-137, the extended form of xylose and the catalytic Mg^{2+} were removed from the figure for clarity. The hydrogen bonds are shown as dashed lines.

et al.[23] have described are the same as our Mg^{2+} or Mn^{2+} sites.

The biochemical results described above are from a variety of microbial sources. The sequences of a number of these enzymes have been determined. When these sequences are aligned the active site of xylose isomerase is found to be highly conserved,[28,43,53] and so should be the mechanism (see Fig. 8). When the crystallographic and biochemical results are compared it becomes clear that the extended form of the sugar is involved in the mechanism, and that His-54 is ideally situated to act as a catalytic base in a ring opening reaction.

Proposed Mechanism

In the conversion of α-D-xylose to α-D-xylulose by xylose isomerase, the enzyme first binds α-D-xylose, then catalyzes a ring opening step, followed by the isomerization step, then catalyzes a ring closing step, and finally the release of the product, α-D-xylulose. The reverse reaction would proceed through the same steps. This mechanism is a further refinement of the mechanism we reported at the American Crystallographic Association Transactions symposium in 1989.[51]

The binding of α-D-xylose to xylose isomerase positions the sugar for the ring opening reaction. As shown in Figure 12, His-54 operates as an acid–base catalyst by shuttling a proton between the O1 hydroxyl and the ring oxygen of α-D-xylose. This suggests that His-54 would be protonated at ND1, and would explain the titration of a proton with a pK_a of 6.5 in the activity vs. pH profile. The removal of the O1 proton by His-54 may be electrostatically facilitated by Asp-57, which is hydrogen bonded to His-54. This portion of the mechanism is similar to the serine proteases, in which a proton is removed from the catalytic serine by the catalytic histidine, and an aspartate electrostatically facilitates this proton transfer.[55,56]

The open form of D-xylose is bound to the enzyme in an extended conformation (see Fig. 7A). Hydrogen bonds between the O3 hydroxyl and Asp-287 and between the O4 hydroxyl and Glu-181 are con-

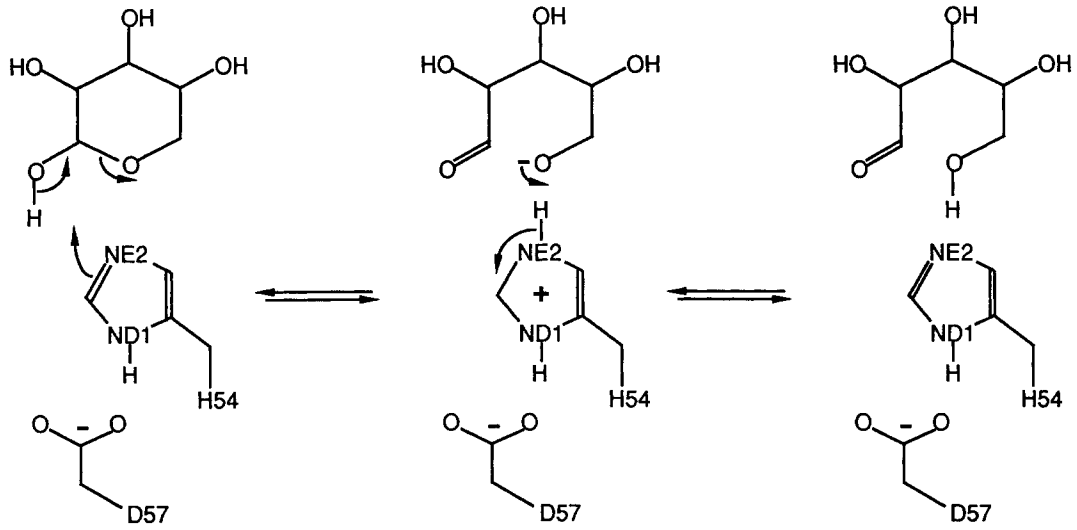

Fig. 12. Schematic diagram of the ring opening reaction in xylose isomerase.

served between the cyclic and extended forms of D-xylose (see Tables VII and VIII). The structural Mn^{2+}, which was displaced by the cyclic α-D-xylose, coordinates to the O2 and O4 of the extended D-xylose. Collyer and Blow have reported the structure of xylose isomerase with the cyclic α-D-glucose analog thio-α-D-glucopyranose (TPG).[26] In contrast to our structure, the TPG binds in the presence of both magnesium ions, suggesting that the structural divalent cation may not be displaced upon binding of α-D-xylose.[26] A water molecule, coordinated to the catalytic Mn^{2+}, and Lys-183 position the sugar such that O1–C1–C2–O2 is in a *cis* conformation, as Schray and Rose[17] predicted.

The isomerization reaction involves the transfer of two hydrogens; the O2 and C2 hydrogens of D-xylose are transferred to the O1 and C1 of D-xylulose. In the initial step in the isomerization, a water molecule, initially hydrogen bonded to the O1 and O2 of the substrate, OD1 of Asp-257 and coordinated to the catalytic Mn^{2+}, transfers a proton to OD1 of Asp-257 to form a hydroxide ion. The hydroxide ion removes the O2 hydroxyl proton of D-xylose, generating a negative charge on the O2 (see Fig. 13). The hydroxide ion and the negative charge on the O2 are stabilized by the catalytic Mn^{2+}. This portion of the mechanism is similar to the staphylococcal nuclease mechanism, in which a Ca^{2+} stabilizes the generation of a hydroxide ion by transferring its proton to Glu 43.[57–59] The catalytic Mn^{2+} moves 1.76 Å to directly coordinate to the O1 and O2 of the sugar, displacing the water molecule carrying the O2 proton. The water molecule is most likely displaced toward Asp-257, which no longer is coordinated to the catalytic Mn^{2+}. The transfer of the C2 hydrogen of D-xylose to the pro-R position on C1 to form D-xylulose is accomplished as a 1,2-hydride shift. Xylose isomerase has evolved to stabilize the transition state of the hydride shift, in which the C2 is principally planar, as seen in the XI–xylose–$MnCl_2$ structure. The negative charge on O2 migrates to the O1 during the hydride shift (see Fig. 13). Finally, a water molecule donates a proton to the O1 to form the O1 hydroxyl of D-xylulose and a hydroxide ion. The OD1 of Asp-257 then transfers a proton to the hydroxide ion. This water molecule (hydroxide ion) need not be the same as the one that extracted the proton from the O2 hydroxyl. Simultaneously, the catalytic Mn^{2+} becomes coordinated to Asp-257 and the water molecule involved in the hydroxyl proton transfer. In the final step the enzyme catalyzes the cyclization of D-xylulose, using the reverse of the ring opening reaction, described above (see Fig. 12). These final steps regenerate the enzyme, allowing the product α-D-xylulose to diffuse out of the enzyme, completing the isomerization reaction.

There are a number of key features of the isomerization reaction: (1) the isomerization reaction uses the open form of the sugar and His-54 acts as a base catalyst in the ring opening and closing steps of the reaction; (2) a water molecule/hydroxide ion transfers the hydroxyl proton (O1 to O2); (3) Asp-257 accepts a proton from a water molecule to form the hydroxide ion; (4) the negative charges on the hydroxide ion and substrate are stabilized by the catalytic Mn^{2+}; and (5) a hydride shift is used to transfer the hydrogen from the C2 to the C1. We have proposed a hydride shift mechanism rather than an acid-base mechanism for the C2–C1 hydrogen transfer for two reasons: First, no suitable base is found in the structures of xylose isomerase that could transfer the C2–C1 proton; and second, the C2–C1 hydrogen does not exchange with solvent.[15,16] In place of a suitable base one finds Trp-16 in the crystal struc-

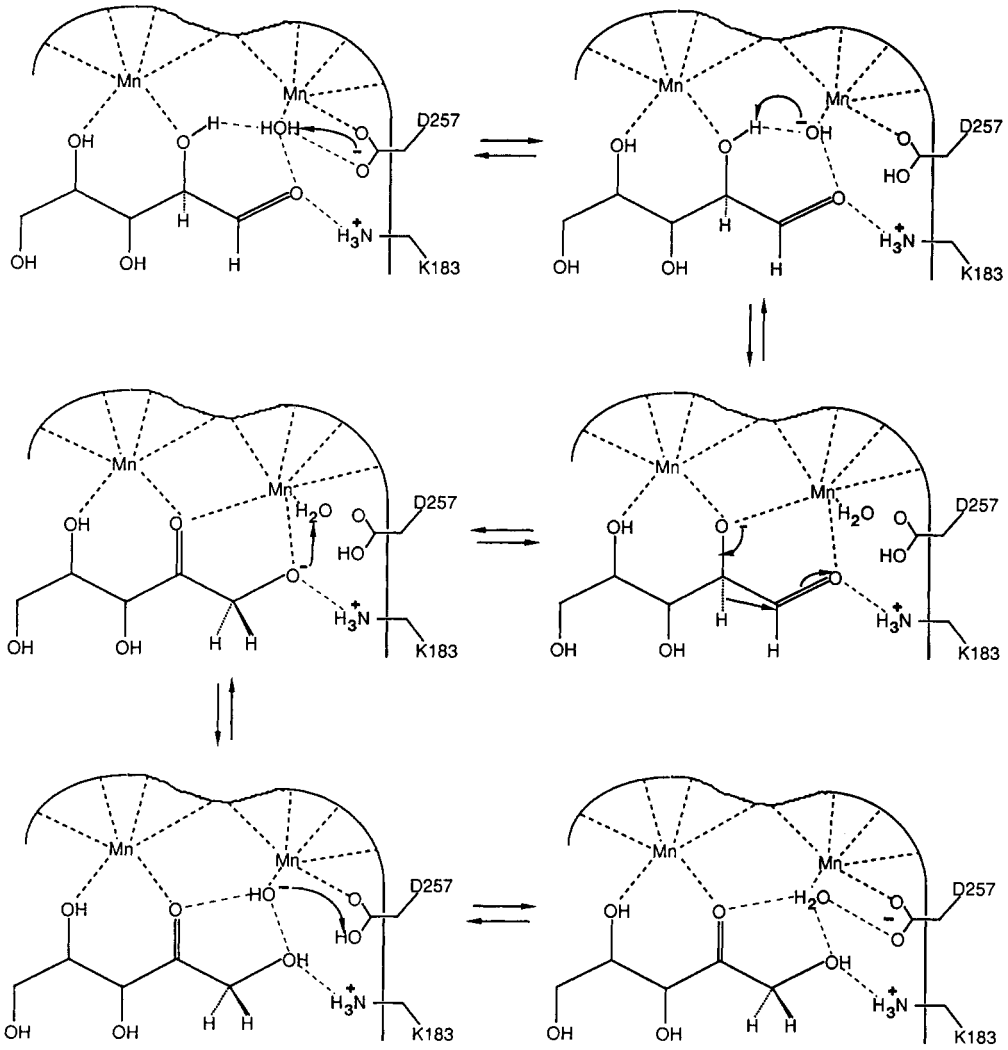

Fig. 13. Schematic diagram of the metal-mediated 1,2-hydride shift reaction in xylose isomerase.

ture, which forms a hydrophobic contact with the substrate in its extended form. Trp-16 excludes solvent from the C1 and C2 of the substrate. This mechanism can be contrasted with the isomerization of dihydroxyacetone phosphate to glyceraldehyde-3-phosphate by triose phosphate isomerase, in which Glu-165 acts as a catalytic base and the C1–C2 hydrogen exchanges with solvent.[60]

Other Work

Finally, we will examine the structural studies of xylose isomerase performed elsewhere. Xylose isomerase structures have been solved by at least five groups (Carrell et al.,[25] Henrick et al.,[43] Farber et al.,[61] Rey et al.,[62] and our group at Genex). The active site of this enzyme is highly conserved throughout the organisms studied, and one would expect few differences in the active sites of these structures. All the residues that we have found to be either involved in the cation binding sites (Glu-181, Asn-215, Glu-217, His-220, Asp-245, Asn-247, Asp-255, Asp-257, Asp-287, or binding the substrate, D-xylose or the competitive inhibitor, xylitol (Trp-16, His-54, Trp-137, Glu-181, Lys-183, Glu-217, Asp-287) are found to be conserved.[28,43,53]

Carrell et al.[27] solved the first structure of xylose isomerase from *Streptomyces rubiginosus* at 4.0 Å, and has recently reported structures at 1.9 Å with xylitol, D-xylose, and a substrate analog that is a suicide inactivator of xylose isomerase.[25] The conformation they describe for the XI–xylitol is very similar to ours, but the XI–xylose structure they describe is considerably different from ours. The D-xylose of Carrell et al.[25] is bound to the enzyme in an extended conformation, but unlike the xylitol structure it binds with its O3 and O5 bound to the structural Mn^{2+} and the C1 in close proximity to the NE2 of His-54. Neither the catalytic Mn^{2+} nor the

conserved Lys-183 is involved in the binding of the D-xylose (see Fig. 1E in Carrell et al.[25]). They propose that His-54 acts as a general base in the transfer of the proton from C2 of D-xylose to C1 D-xylulose. We believe that if this were the case, the proton would show exchange with solvent shown in their Figure 1E. Collyer and Blow[26] believe that Carrell et al.,[25] like we, have obtained a mixture of the cyclic and extended forms of D-xylose.

Farber et al.[45] solved the structure of the enzyme from *Streptomyces olivochromogenes* by MIR at 3.0 Å. Using a flow cell, they were the first to show the binding of a cyclic D-xylose, and propose that His-54 and Asp-57 are involved in a ring opening.[53] They were first to recognize that the mechanism of xylose isomerase may involve a hydride shift, but at 3.0 Å were not able to propose a detailed mechanism. In addition, they have collected native and Eu-derivative data to 3.0 Å using the Laue method.[61] The difference map clearly showed two Eu atoms bound in the active site.

Henrick et al.[43,46] have determined the structure of XI from *Arthrobacter* B3728 by MIR at 2.3 Å resolution. They have given a detailed description of this enzyme and its complex with the inhibitor D-sorbitol.[43] D-Sorbitol is to D-glucose what xylitol is to D-xylose. Their D-sorbitol structure is similar to our xylitol structure, with one difference: they find only one metal ion that corresponds to our structural Mn^{2+}. Their crystals are grown in the presence of 10 mM $MgCl_2$.[63] Since Mg^{2+} has only 10 electrons, the catalytic Mg^{2+} could have been interpreted as a water molecule, due to its nonideal geometry (see Table VI). Recently, they have suggested that the absence of the catalytic Mg^{2+} is probably a pH effect.[52] Henrick et al.[43] suggest that His-220 (His-219 in their structure) might serve as the general base in its isomerization. But in our structures and in the Carrell et al.[25] structures the conserved His-220 is bound to the catalytic Mn^{2+}. The most recent paper of Collyer and Blow[26] explains how the results of Carrell et al.[25] are consistent with a hydride shift mechanism. In order to do so they suggest that Carrell et al.[25] have a mixture of conformations in their XI–xylose structure (see above).

Note Added

The day before we submitted this manuscript, Collyer et al.[52] published a paper describing the identical mechanism of D-xylose isomerase. They reported on 22 structures of the *Arthrobacter* strain B3728 D-xylose isomerase complexed with a variety of metals, substrates, and inhibitors at 2.3–2.7 Å resolution. We were able to unravel the same mechanism using only five structures, the key being that our structures were done at much higher resolution (1.6–1.7 Å). The higher resolution allowed us to identify an alternative position of the catalytic manganese in the presence of D-xylose. Collyer et al.[52] suggested that Asp-255 is repositioned when the catalytic manganese is coordinated to both the O1 and O2 of the substrate. We do not observe an alternate position for Asp-255 in the XI–xylose–$MnCl_2$ structure, which has an alternate position for the catalytic manganese (see Fig. 10B). However, if the occupancy of the alternative position of Asp-255 were the same as the occupancy of the alternate position for the catalytic manganese (0.18), we would have difficulty seeing it. Like Collyer et al.,[52] we do see an alternate position for Asp-255 in the XI–xylitol structure (see Fig. 10A). A detailed molecular mechanics study of these alternative positions should clarify these details of the mechanism.

CONCLUSIONS

The binding of sugars to xylose isomerase from *Streptomyces rubiginosus* is similar to that found in the sugar binding proteins.[49] The similarities include networks of cooperative hydrogen bonds and an aromatic residue interacting with the hydrophobic portion of the sugar.[50] Xylose isomerase is unique in that it binds an open form of D-xylose and divalent metal ions are directly coordinated to the open form of the sugar.

We have proposed a detailed metal-mediated hydride shift mechanism for xylose isomerase. It accounts for the majority of xylose isomerase's biochemical properties, including (1) the lack of solvent exchange between the 2-position of D-xylose and the 1-pro-R position of D-xylulose, (2) the chemical modification data of histidine and lysine, (3) the pH vs. activity profile, and (4) the role of the two metal ions in the mechanism. Other mechanisms for this enzyme could be envisioned, but none of the others set forth to date accounts for these four observations.

ACKNOWLEDGMENTS

We would like to thank Drs. H. L. Carrell, A. Glasfeld, and C. Collyer for a preprint of their most recent papers: Carrell et al.,[25] Farber et al.,[53] and Henrick et al.,[43] respectively. We would like to thank Drs. R. Drummond, K. Hardman, J. Hautala, and R. Raag and the reviewers of this manuscript for their useful comments and Cetus Corporation for its support of this work.

REFERENCES

1. Hochster, R.M., Watson, R.W. Xylose isomerase. J. Am. Chem. Soc. 75:3284–3285, 1953.
2. Hochster, R.M., Watson, R.W. Enzymatic isomerization of D-xylose to D-xylulose. Arch. Biochem. Biophys. 48:120–129, 1954.
3. Bucke, C., Wiseman, A. eds. Industrial glucose isomerase. In: "Topics in Enzyme and Fermentation Biotechnology," Part b. Chichester: Halstead Press, 1977: 147–171.
4. Layman, P.L. Industrial enzymes battling to remain specialties. Chem. Eng. News 64(37):11–14, 1986.
5. Sfiligoj, E. HFCS: Riding high as per caps climb. Beverage Ind. June:62, 1989.
6. Hogue-Angeletti, R.A. Subunit structure and amino acid composition of xylose isomerase from *Streptomyces albus*. J. Biol. Chem. 250:7814–7818, 1975.
7. Lobry de Bruyn, C.A., Alberda van Ekenstein, W. Action

des alcalis sur les sucres, II Rec. Trav. Chim. 14:195–207, 1895.
8. Lobry de Bruyn, C.A., Alberda van Ekenstein, W. Action des alcalis sur les sucres. IV & VI Rec. Trav. Chim. 16: 241–244, 256–263, 1897.
9. Speck, J.C. Lobry de Bruyn–Alberda van Ekenstein transformation Adv. Carbohydrate Chem. 13:63–103, 1958.
10. Wohl, A., Neuberg, C. Zur kenntniss des glycerin-aldehyds. Ber. 33:3095–3110, 1900.
11. Topper, Y.J., Stetten, D., Jr. The alkali-catalyzed conversion of glucose into fructose and mannose. J. Biol. Chem. 189:191–202, 1951.
12. Gleason, W.B., Barker, R. Evidence for a hydride shift in the alkaline rearrangements of D-ribose. Can. J. Chem. 49:1433–1440, 1971.
13. Harris, D.W., Feather, M.S. Studies on the mechanism of the interconversion of D-glucose, D-mannose and D-fructose in acid solution. J. Am. Chem. Soc. 97:178–181, 1975.
14. Ramchander, S., Feather, M.S. An intramolecular C-2 → C-1 hydrogen transfer during the acid-catalyzed conversion of D-xylose to D-*threo*-pentulose (D-xylulose). Arch. Biochem. Biophys. 178:576–580, 1977.
15. Rose, I.A., O'Connell, E.L., Mortlock, R.P. Stereochemical evidence for a cis-enediol intermediate in Mn-dependent aldose isomerases. Biochim. Biophys. Acta 179:376–379, 1969.
16. Bock, K.B., Meldal, M., Meyer, B., Wiebe, L. Isomerization of D-glucose with glucose isomerase. A mechanistic study, Acta Chem. Scand. B37:101–108, 1983.
17. Schray, K.J., Rose, I.A. Anomeric specificity and mechanism of two pentose isomerases. Biochemistry 10:1058–1062, 1972.
18. Makkee, M., Kieboom, A.P.G., van Bekkum, H. Glucose-isomerase-catalyzed D-glucose-D-fructose interconversion: Mechanism and reactive species. Recl. Trav. Chem. Pays-Bas 103:361–364, 1984.
19. Callens, M., Kersters-Hilderson, H., Van Opetal, O., De Bruyne, C.K. Catalytic properties of D-xylose isomerase from *Streptomyces violaceoruber*. Enzyme Microb. Technol. 8:696–700, 1986.
20. Hoschle, A., Balogh, K., Laszio, E., Hollo, J. Determination of functional groups in glucose isomerase. Starch/Starke 36:26–30, 1984.
21. Danno, G. Studies on D-glucose-isomerizing enzyme from *Bacillus coagulans*, strain HN-68. Part V. Comparative study on the three activities of D-glucose, D-xylose and D-ribose isomerization of crystalline enzyme. Agr. Biol. Chem. 34:1805–1814, 1970.
22. Danno, G. Studies on D-glucose-isomerizing enzyme from *Bacillus coagulans*, strain HN-68. Part VI. The role of metal ions on isomerization of D-glucose and D-xylose by the enzyme. Agr. Biol. Chem. 35:997–1006, 1971.
23. Callens, M., Kersters-Hilderson, H., Vangrysperre, W., De Bruyne, C.K. Catalytic properties of D-xylose isomerase from *Streptomyces violaceoruber*. Enzyme Microb. Technol. 10:695–700, 1988.
24. Callens, M., Tomme, P., Kersters-Hilderson, H., Cornelis, R., Vangrysperre, W., De Bruyne, C.K. Metal ion binding to D-xylose isomerase from *Streptomyces violaceoruber*. Biochem. J. 250:285–290, 1988.
25. Carrell, H.L., Glusker, J.P., Burger, V., Manfre, F., Tritsch, D., Biellmann, J.-F. X-ray analysis of D-xylose isomerase at 1.9Å: Native enzyme in complex with substrate and with a mechanism-designed inactivator. Proc. Natl. Acad. Sci. U.S.A. 86:4440–4444, 1989.
26. Collyer, C.A., Blow, D.M. Observations of reaction intermediates and the mechanism of aldose-ketose interconversion by D-xylose isomerase. Proc. Natl. Acad. Sci. U.S.A. 87:1362–1366, 1990.
27. Carrell, H.L., Rubin, B.H., Hurley, T.J., Glusker, J.P. X-ray crystal structure of D-xylose isomerase at 4-Å resolution. J. Biol. Chem. 259:3230–3236, 1984.
28. Wong, H.C., Ting, Y., Myambo, K., Watt, K.W., Toy, P.L., Drummond, R.J. Xylose isomerase gene from *Streptomyces rubiginosus:* Molecular cloning, sequencing and expression of the structural gene. Nucleic Acids Res., 1989, submitted.
29. Gilliland, G.L., Davies, D.R. Protein crystallization: The growth of large-scale single crystals. Methods Enzymol 104:370–381, 1984.
30. Howard, A.J., Gilliland, G.L., Finzel, B.C., Poulos, T.L., Ohlendorf, D.H., Salemme, F.R. Use of an imaging proportional counter in macromolecular crystallography. J. Appl. Crystallogr. 20:383–387, 1987.
31. Hull, S.R., Stewart, J.M., Munn, R.J. XTAL: New concepts in program system design. Acta Crystallogr. A36: 379–989, 1980.
32. Jones, T.A. A graphics model building and refinement system for macromolecules. J. Appl. Crystallogr. 11:268–272, 1978.
33. Hendrickson, W.A., Lattman, E.E. Representation of phase probability distributions for simplified combination of independent phase information. Acta. Crystallogr. B26: 136–143, 1970.
34. Hendrickson, W.A., Wyckoff, H.W., Hirs, C.H.W., Timasheff, S.N., eds. Stereochemically restrained refinement of macromolecular structures. Methods Enzymol. 115:252–270, 1985.
35. Finzel, B.C., Incorporation of fast Fourier transforms to speed restrained least-squares refinement of proteins. J. Appl. Crystallogr. 20:53–55, 1987.
36. Agarwal, R.C. A new least-squares refinement technique based on the fast Fourier transform algorithm. Acta Crystallogr. A34:791–809, 1978.
37. Agarwal, R.C. New results on fast Fourier least-squares refinement technique. In: "Refinement of Protein Structures, Proceedings of the Daresbury Conference," Daresbury Lab. UK, 1980:24–28.
38. Bernstein, F.C., Koetzle, T.F., Williams, G.J., Meyer, E.E.J., Brice, M.D., Rodgers, J.R., Kennard, O., Shimanouchi, T., Tsumi, M. The protein data bank: a computer-based archival file for macromolecular structures. J. Mol. Biol. 112:535–542, 1977.
39. Schray, K.J., Mildvan, A.S. Kinetic and magnetic resonance studies of the mechanism of D-xylose isomerase. J. Biol. Chem. 247:2031–2037, 1972.
40. Mavridis, I.M., Hatada, M.H., Tulinsky, A., Lebioda, L. Structure of 2-keto-3-deoxy-6-phosphogluconate aldolase at 2.8 Å resolution. J. Mol. Biol. 152:419–444, 1982.
41. Banner, D.W., Bloomer, A.C., Petsko, G.A., Phillips, D.C., Pogson, C.I., Wilson, I.A., Corran, P.H., Furth, A.J., Milman, J.D., Offord, R.E., Priddle, J.D., Waley, S.G. Structure of chicken muscle triose phosphate isomerase determined crystallographically at 2.5 Å resolution using amino acid sequence data. Nature (London) 255:609–614, 1975.
42. Stuart, D.I., Levine, M., Muirhead, H., Stammers, D.K. Crystal structure of cat muscle pyruvate kinase at a resolution of 2.6 Å J. Mol Biol. 134:109–142, 1979.
43. Henrick, K., Collyer, C.A., Blow, D.M. Structures of D-xylose isomerase from *Arthrobacter* strain B3728 containing the inhibitors xylitol and D-sorbitol at 2.5Å and 2.3Å resolution, respectively. J. Mol. Biol. 208:129–157, 1989.
44. Lesk, A.M., Branden, C., Chothia, C. Structural principles of α/β barrel proteins: The packing of the interior of the sheet. Proteins 5:139–148, 1989.
45. Farber, G.K., Petsko, G.A., Ringe, D. The 3.0 Å crystal structure of xylose isomerase from *Streptomyces olivochromogenes*. Protein Engineer. 1:459–466, 1987.
46. Henrick, K., Blow, D.M., Carrell, H.L., Glusker, J.P. Comparison of backbone structures of glucose isomerase from *Streptomyces* and *Arthrobacter*. Protein Engineer. 1:467–469, 1987.
47. Hardman, K.D., Agarwal, R.C., Freiser, M.J. Manganese and calcium binding sites of concanavalin A. J. Mol. Biol. 157:69–86, 1982.
48. Young, J.M., Schray, K.J., Mildvan, A.S. Proton magnetic relaxation studies of the interaction of D-xylose and xylitol with D-xylose isomerase. J. Biol. Chem. 250:9021–9027, 1975.
49. Quiocho, F.A. Carbohydrate-binding proteins: Tertiary structures and protein-sugar interactions. Annu. Rev. Biochem. 55:287–315, 1986.
50. Quiocho, F.A., Sack, J.S., Vyas, N.K. Stabilization of charges on isolated ionic groups sequestered in proteins by polarized peptide units. Nature (London) 329:561–564, 1987.
51. Whitlow, M., Howard, A.J. 1.6Å Structures of xylose isomerase from *Streptomyces rubiginosus* with xylitol and

xylose and their mechanistic implications. Transact. Am. Crystallogr. Assoc. 25:in press, 1989.
52. Collyer, C.A., Henrick, K., Blow, D.M. Mechanism for aldose-ketose interconversion by D-xylose isomerase involving ring opening followed by a 1,2-hydride shift. J. Mol. Biol. 212:211–235, 1990.
53. Farber, G.K., Glasfeld, A., Tiraby, G., Ringe, D., Petsko, G.A. Crystallographic studies of the mechanism of xylose isomerase. Biochemistry 28:7289–7297, 1989.
54. Sowden, J.C., Schaffer, R. The isomerization of D-glucose by alkali in D_2O at 25°. J. Am. Chem. Soc. 74:505–507, 1952.
55. Blackburn, S. Chymotrypsin: charge-relay system. In: "Enzyme Structure and Function." New York: Marcel Dekker, 1976: 62–68.
56. Warshal, A., Naray-Szabo, G., Sussman, F. and Hwang, J.-K. How do serine proteases really work? Biochemistry 28:3629–3638, 1989.
57. Cotton, F.A., Hazen, E.E., Jr., Legg, M.J. Staphylococcal nuclease: Proposed mechanism of action based on structure of enzyme-thymidine 3′,5′-bisphosphate-calcium ion complex at 1.5-Å resolution. Proc. Natl. Acad. Sci. U.S.A. 76:2551–2555, 1979.
58. Serpersu, E.H., Shortle, D., Mildvan, A.S. Kinetic and magnetic resonance studies of active-site mutants of staphylococcal nuclease: Factors contributing to catalysis. Biochemistry 26:1289–1300, 1987.
59. Åqvist, J., Warshal, A. Calculations of free energy profiles for the staphylococcal nuclease catalyzed reaction. Biochemistry 28:4680–4689, 1989.
60. Alber, T., Banner, D.W., Bloomer, A.C., Petsko, G.A., Phillips, D., Rivers, P.S., Wilson, I.A. On the three-dimensional structure and catalytic mechanism of triose phosphate isomerase. Phil. Trans. R. Soc. London B293, 159–171, 1981.
61. Farber, G.K., Machin, P., Almo, S.C., Petsko, G.A., Hajdu, J. X-ray Laue diffraction from crystals of xylose isomerase. Proc. Natl. Acad. Sci. U.S.A. 85:112–115, 1988.
62. Rey, F., Jenkins, J., Janin, J., Lasters, I., Alard, P., Claessens, M., Matthyssens, G., Wodak, S. Structural analysis of the 2.8Å model of xylose isomerase from *Actinoplanes missouriensis*. Proteins: Struct., Funct. Genet. 4:165–173, 1988.
63. Atkins, J., Brick, P., Jones, H.B., Hirayama, N., Shaw, P.-C., Blow, D.M. The crystallization of glucose isomerase from *Arthrobacter* B3728. Biochem. Biophys. Acta 874: 375–377, 1986.